Stable Isotope-Based Paleoaltimetry

David B. Rowley[1] and Carmala N. Garzione[2]

[1]Department of the Geophysical Sciences, The University of Chicago, Chicago, Illinois 60637; email: drowley@uchicago.edu

[2]Department of Earth and Environmental Sciences, University of Rochester, Rochester, New York 14627

Annu. Rev. Earth Planet. Sci. 2007. 35:463–508

First published online as a Review in Advance on January 29, 2007

The *Annual Review of Earth and Planetary Sciences* is online at earth.annualreviews.org

This article's doi:
10.1146/annurev.earth.35.031306.140155

0084-6597/07/0530-0463$20.00

Key Words

paleoelevation, stable isotopes, Tibet, Andes, plateaus

Abstract

The quantitative estimation of paleoaltitude has become an increasing focus of Earth scientists because surface elevation provides constraints on the geodynamic mechanisms operating in mountain belts, as well as the influence of mountain belt growth on regional and global climate. The general observation of decreasing $\delta^{18}O$ and $\delta^{2}H$ values in rainfall as elevation increases has been used in both empirical and theoretical approaches to estimate paleoelevation. These studies rely on the preservation of ancient surface water compositions in authigenic minerals to reconstruct the elevation at the time the minerals were forming. In this review we provide a theory behind the application of stable isotope-based approaches to paleoaltimetry. We apply this theory to test cases using modern precipitation and surface water isotopic compositions to demonstrate that it generally accords well with observations. Examples of the application of paleoaltimetry techniques to Himalaya-Tibet and the Andes are discussed with implications for processes that cause surface uplift.

INTRODUCTION

The recent books *Tectonic Uplift and Climate Change* (Ruddiman 1997) and *Tectonic Boundary Conditions for Climate Reconstructions* (Crowley & Burke 1998) emphasize the importance of reconstructing paleoaltimetry. A review by Chase et al. (1998) provides the baseline against which to measure significant progress in this area of research in the past eight years. In their review of paleoaltimeters available at that time, Chase et al. (1998) noted the potential of stable isotopes but commented that a coherent theory behind these estimates did not exist. The past eight years has also witnessed continued developments based on other approaches. Our list below is not comprehensive, but simply provides evidence that the community has taken up this challenging problem with considerable creativity and hence we can anticipate many new developments in the near future. Two other quantitative approaches to paleoaltimetry that were outlined and reviewed by Chase et al. (1998) include use of foliar physiognomy (*a*) to use the difference in mean annual temperature estimates of a coastal and potentially elevated inland site and an assumed lapse rate (Gregory-Wodzicki 2000) or (*b*) to use the difference in enthalpy between a coastal and potentially elevated inland site at the same (paleo)latitude to estimate altitude (Forest et al. 1999, Spicer et al. 2003). Both of these approaches derive from the correlation of various physiognomic characteristics of modern floras to modern climate parameters (Forest et al. 1999, Gregory 1994, Wolfe 1993). To apply these techniques to the past it is necessary to assume that precisely the same correlation exists for the paleofloras, which is hard to assess quantitatively. In a third approach, Sahagian & Maus (1994) suggested that the vesicularity of basalts correlated with atmospheric pressure. Their analysis suggests an altitude $\pm 1\sigma$ error of 0.1 bar or approximately 1 to 1.4 km. Sahagian et al. (2002) have improved techniques for estimating vesicle size distributions, and they applied this approach to the western United States. McElwain (2004) and Beerling & Royer (2002) have adopted the stomatal index approach for estimating paleo-P_{CO_2} to paleoaltimetry by recognizing the exponential decrease of P_{CO_2} with elevation. In addition, cosmogenic nuclide approaches to estimating paleoelevations continue to garner considerable interest. Estimated uncertainties are comparable among these methods, but their applicability in the geologic past is quite variable. Both enthalpy and mean annual temperature differences require angiosperm floras. One would presume that the correlation of physiognomic characteristics to climate parameters will be increasingly influenced by evolutionary factors and hence that such estimates would become increasingly uncertain with geologic age. Irrespectively, these techniques are only applicable to the past 100 Ma or so. High altitude basalts, usually erupted as volcanoes above the mean surface, have fairly limited preservation potential, and hence limited applicability to the geologic past. By contrast, intermontane basins are widely preserved in the geologic past, and various sediments, including lacustrine carbonates, soil carbonates, fossil cellulose, fish teeth and otoliths, mammal teeth, and select clays, may retain records of fossil $\delta^{18}O_p$ or δ^2H_p, providing the materials necessary for estimating elevation over a considerable interval of the past.

In this review, we focus almost entirely on stable isotope-based approaches to paleoaltimetry. We provide a coherent theory behind the application of stable

isotope-based approaches to paleoaltimetry and demonstrate that observations from surface rainfall and surface water isotopic composition generally agree with the theory. We also review several examples of the application of this approach to estimate paleoelevations in the Himalayas (Garzione et al. 2000a,b; Rowley et al. 2001), Tibet (Currie et al. 2005, Cyr et al. 2005, Rowley & Currie 2006), and the Andes (Garzione et al. 2006). In addition, we review the newly developed Δ_{47} approach to stable isotope-based thermometry and its application to paleoaltimetry, based on the Andes (Ghosh et al. 2006b).

The principles behind stable isotope-based paleoaltimetry were established in studies that observed large fractionations in the H and O isotopes in atmospheric water vapor, rainfall, and snowfall associated with increasing elevation (e.g., Ambach et al. 1968, Siegenthaler & Oeschger 1980, Rozanski & Sonntag 1982, Gonfiantini et al. 2001). The primary fractionation mechanism results from the adiabatic expansion of water vapor as it ascends a mountain slope, which causes cooling and condensation. The condensation and subsequent rainout of water as rain or snow causes heavy isotopes of ^{18}O and ^{2}H (D) to be removed from the remaining vapor because heavy isotopes form stronger bonds and are therefore less likely to break during equilibrium water-vapor transformation. The following section discusses the thermodynamics behind this fractionation process and describes a simple model that reflects the observed changes in meteoric water with increasing altitude.

ATMOSPHERIC THERMODYNAMICS OF OXYGEN AND HYDROGEN ISOTOPE-BASED ESTIMATES OF ELEVATION FROM OROGRAPHIC PRECIPITATION

Rowley et al. (2001) presented a model that theoretically predicts the expected relationship between elevation and stable isotopic composition of precipitation. We outline this simple parcel-based model that tracks the moist static energy, water vapor content, and water vapor and condensate isotopic composition along ascending, precipitating trajectories. The output of this model is the expected systematic behavior of the oxygen and hydrogen isotopic composition of precipitation as a function of elevation. In this discussion, we employ $\Delta(\delta^{18}O)$ and $\Delta(\delta^{2}H)$, the difference in isotopic composition between a low, preferably near sea level, composition and a potentially elevated sample as the monitor of elevation, recognizing that this difference, rather than the absolute isotopic composition, is a measure of elevation.

The Model

At equilibrium, there is a fractionation of ^{18}O relative to ^{16}O and ^{2}H relative to ^{1}H that occurs as water vapor condenses to form precipitation (rain or snow). The magnitude of fractionation is determined by the equilibrium fractionation factor, α, which, for oxygen, is defined as

$$\alpha_O = R_p/R_v = (\delta^{18}O_p + 1000)/(\delta^{18}O_v + 1000),$$

where R_p is the ratio of $^{18}O/^{16}O$ in precipitation and R_v is the ratio of $^{18}O/^{16}O$ in water vapor. The quantities $\delta^{18}O_p$ and $\delta^{18}O_v$ are the ratios in precipitation and vapor, respectively, relative to a standard [standard mean ocean water (SMOW)] expressed as per mil (‰), such that, for oxygen:

$$\delta^{18}O_p = (R_p/R_{SMOW} - 1) * 1000.$$

Substitution of ^2H and ^1H for ^{18}O and ^{16}O, respectively, in the above results in the identical relations for $^2H/^1H$ fractionation. The fractionation factor, α, is a function of the temperature at which the phase transformation takes place and the phases involved. In the atmosphere, fractionation occurs between water vapor and liquid water or between water vapor and water ice. The temperature dependence of $\alpha(T)$ has been determined experimentally for liquid-vapor equilibrium (Horita & Wesolowski 1994, Majoube 1971a) and for ice-vapor equilibrium (Majoube 1971b, Merlivat & Nief 1967). Existing experimental results are in very close agreement and we use the following relations for oxygen:

$$1000 \ln \alpha_O(T)_{l-v} = -7.685 + 6.7123(10^3T^{-1}) - 1.6664(10^6T^{-2}) + 0.35041(10^9T^{-3})$$
$$\text{and} \quad 1000 \ln \alpha_O(T)_{i-v} = 11839/T - 28.224,$$

and for hydrogen isotopes:

$$1000 \ln \alpha_H(T)_{l-v} = 1158.8 * 10^{-9}T^3 - 1620.1 * 10^{-6}T^2 + 794.84 * 10^{-3}T - 161.09 + 2.9992 * 10^9T^{-3} \quad \text{and}$$
$$1000 \ln \alpha_H(T)_{i-v} = 16288/T^2 * 10^3 - 93.4,$$

where T is the temperature in Kelvin and α_O and α_H with subscripts l, v, and i are liquid, vapor, and ice of oxygen and hydrogen isotopes, respectively. Because liquid water can be cooled below the freezing temperature of water by 20 K or more, there is not an abrupt step in α_O or α_H at 273.15 K. Thus, for temperatures between 273.15 K and 253.15 K, we mix between ice and liquid water fractionation. At any given T, the equilibrium isotopic compositions of oxygen and hydrogen in precipitate ($\delta^{18}O_p$ or δ^2H_p) and vapor ($\delta^{18}O_v$ or δ^2H_v) are described by the following relations:

$$\delta^{18}O_p = \alpha_O(T) * (\delta^{18}O_v + 1000) - 1000 \quad \text{and}$$
$$\delta^2H_p = \alpha_H(T) * (\delta^2H_v + 1000) - 1000.$$

Rayleigh condensation treats the isotopic composition as an open system distillation in which precipitation is successively removed from the vapor as it condenses, leaving the residual vapor progressively depleted in ^{18}O and ^2H. We use $\zeta = -\ln(p/p_S)$ as our vertical coordinate, where p is ambient pressure and p_S is the surface pressure at sea level. The distillation process can then be expressed by the differential equation:

$$\frac{dR_v}{d\zeta} = \frac{dR_p}{d\zeta} = R_v(\alpha(T) - 1)\frac{1}{q}\frac{dq}{d\zeta}, \quad (1)$$

where R_p and R_v are the isotopic ratios in the incremental precipitation and the vapor, respectively; q is the mass mixing ratio of water; and $dq/d\zeta$ is the amount of water condensed from the air parcel to maintain saturation as a consequence of adiabatic

ascent. From atmospheric thermodynamics, it is possible to determine $dq/d\zeta$ with three basic equations:

$$\frac{dz}{d\zeta} = \frac{RT}{g}, \tag{2}$$

where z is altitude in meters and R (without any subscripts) is the gas constant for air ($R = 287\ J\ kg^{-1}\ K^{-1}$). The change in temperature with height depends on whether condensation is occurring, and for rapidly ascending, thermally isolated parcels is described by the relations

$$\frac{dT}{d\zeta} = \frac{RT + Lq_s}{C_p + Lq_s(\ln(e_s))'} \quad \text{if moisture is condensing} \tag{3a}$$

$$\frac{dT}{d\zeta} = -\frac{R}{C_p}T \quad \text{if noncondensing } (q < q_S), \tag{3b}$$

where C_p is the heat capacity of air ($1004.0\ J\ kg^{-1}\ K^{-1}$); q_S is the saturation mass mixing ratio of water ($\approx .622\ e_S/p$); e_S is $e_S(T)$, which is the saturation vapor pressure of water as a function of T based on the Smithsonian meteorological tables; and L is the latent heat contribution owing to condensation, which also varies as a function of T. Equation 3b is the formula for the dry adiabat. Equation 3a incorporates the change in saturation vapor pressure with temperature through the expression

$$(\ln(e_s))' = \frac{1}{e_s}\frac{de_s}{dT}$$

Finally, the amount of water condensed from the air parcel as ice or liquid to maintain saturation is determined through the relation

$$\frac{1}{q}\frac{dq}{d\zeta} = 1 + (\ln(e_s))'\frac{dT}{d\zeta} \quad \text{if condensing } (q \geq q_S) \tag{4a}$$

$$\frac{1}{q}\frac{dq}{d\zeta} = 0 \quad \text{if noncondensing } (q < q_S). \tag{4b}$$

If there is no condensation, q is conserved following the air parcel.

The above calculation takes as initial conditions the temperature (T) and relative humidity (RH), which determine the water vapor concentration of the starting air mass. As illustrated in **Figure 1**, focusing only on oxygen isotopes, air starting at the ground with a specific T and RH is lifted along the dry adiabat following Equations 3b and 4b, with the vapor fraction equal to 1.0 until condensation starts at the cloud condensation level, when $q = q_S$. Condensation then occurs at all levels above the cloud condensation level as described by Equations 3a and 4a, resulting in progressive decrease in the remaining vapor fraction as a function of adiabatic ascent. Latent heat release associated with condensation changes the temperature lapse rate to a moist adiabat, and it is this temperature and the associated phase(s) that control the equilibrium fractionation between the remaining vapor and condensate, as represented by the corresponding αs. This thermodynamically determined adiabatic lapse rate depends solely on the starting T and RH. Therefore, different starting conditions appropriate to different starting air mass conditions will yield different rates of condensation with elevation, and hence $\delta^{18}O$ (δ^2H) versus altitude relationships. The decreasing water

Figure 1

Relationship between temperature, vapor fraction, and normalized isotopic composition of vapor and resultant condensate as a function of elevation for an air parcel that starts at the ground with T = 295 K and RH = 80% and is lifted adiabatically according to the model.

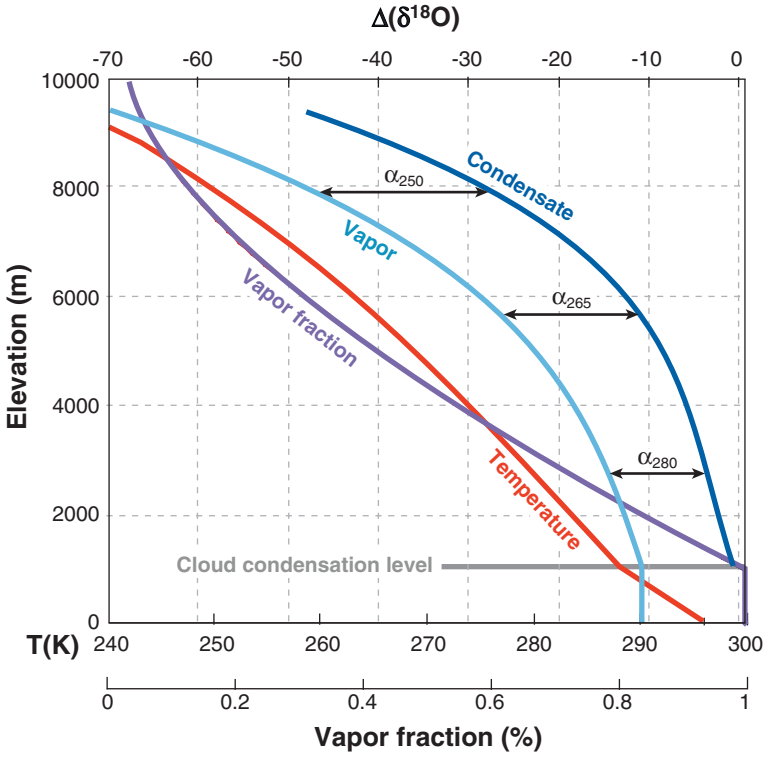

vapor fraction, and hence decreasing ratio of initial to remaining water vapor, with height results in a decrease in the latent heat contribution. Together they drive the Rayleigh distillation process and result in the progressive isotopic depletion of the remaining reservoir from which subsequent condensation occurs.

The model explicitly calculates the equilibrium isotopic composition of the condensate as a function of elevation. However, what we are interested in is the isotopic composition of precipitation that falls to the ground. The transformation of condensate into precipitation is a complex process that is well beyond the scope of the present paper. For our purposes, we adopt the empirical approach used by Rowley et al. (2001) (**Supplementary Figure 1**, follow the Supplemental Material link from the Annual Reviews home page at **http://www.annualreviews.org**). The best fit to the compositions observed at Alpine stations (**Supplementary Figure 1**) is provided by the model in which the precipitation reaching the ground is derived from a mean altitude of 1500 m above the surface from a column thickness of 1,000 m. This scheme for modeling the isotopic composition of precipitation is employed in all other regions. Comparison of model predictions applying this scheme with modern isotopic compositions of precipitation from other regions demonstrates that the scheme yields quite reasonable fits without adjustment (see below). However, it should always be made clear that many regions, particularly those regions where significant

evaporation occurs during precipitation descent from the level of condensation to the ground, will not be fit by this relationship. In the modern world, this is readily tested using deviations of precipitation from the global meteoric water line (GMWL) (Craig 1961, Dansgaard 1964) and particular care needs to be taken in applying this or any Rayleigh distillation-based approach in such regions. The GMWL is the correlation of ^{18}O relative to ^{2}H of precipitation in which the slope of the correlation is primarily controlled by the relative equilibrium fractionation factors and the ^{18}O intercept is kinetically controlled by fractionation from seawater (Craig 1961, Craig & Gordon 1965).

The thermodynamic model that determines the theoretical $\delta^{18}O$ ($\delta^{2}H$) versus altitude relationship is mathematically one-dimensional, in that the equations need only be integrated with respect to ζ. However, the vertical trajectories themselves can wander horizontally in an arbitrarily complex way as the parcel ascends. The chief physical assumption is that the air parcel remains relatively isolated from the surrounding air. Although turbulence, among other processes, no doubt contributes to isotopic lapse rates for precipitation in orographic settings, the close fit of observed isotopic lapse rates with model predictions implies that the model captures the main features determining the relationship between elevation and isotopic composition in low- to intermediate-latitude settings. Note that in the case of estimating the effects of altitude on the isotopic composition of precipitation, the model only needs to be valid for trajectories that produce precipitation. It need not reproduce the observed temperature and water vapor profiles everywhere.

The T and RH of the starting air parcels are the primary determinants of the relationship between elevation (z), $\Delta(\delta^{18}O_p)$, and $\Delta(\delta^{2}H_p)$. Because T and RH vary continuously at the present time, and they certainly varied in the past, Rowley et al. (2001) used modern data on T and RH from low-latitude ($<35^{\circ}$), entirely oceanic regions in the NCEP reanalysis output (Kalnay et al. 1996) to compute the probability density function (pdf) of T and RH as input for the model (**Supplemental Figure 2**).

Each starting T and RH gives rise to a different vertical trajectory through T and vapor fraction space (**Figure 2**), and hence to different isotopic compositions as a function of altitude. Sampling from the pdf of surface T and RH via 1000-iteration Monte Carlo simulation allows determination of the vertical array of pdfs of condensation-weighted mean temperature and vapor fraction (VF) as a function of elevation (**Figure 2**). It is important to note that at each level there is a limited range of T and VF that contributes to the Rayleigh distillation process. The dark blue line in **Figure 2** highlights the modal T and VF as a function of elevation from the surface T and RH. If we now add isotopic composition of modeled precipitation as a function of elevation to the analysis we see the respective contributions of starting T and RH on the isotopic composition as a function of elevation, as shown in **Figure 3**. Note that the isotopic lapse rate (‰/meter) is the inverse of the graph in **Figure 3**. The heavy dark blue curve shows the mean predicted isotopic composition of precipitation as a function of elevation that corresponds with a starting surface T of 295 K and RH of 80%, which is the mean of the modern-day T and RH pdf. Other curves show model output for conditions that are approximately $\pm 1\sigma$ and $\pm 2\sigma$ in T and $\pm 2\sigma$ in RH. These correspond with ± 4 K and ± 8 K in T and $\pm 8\%$ in RH. From **Figure 3**,

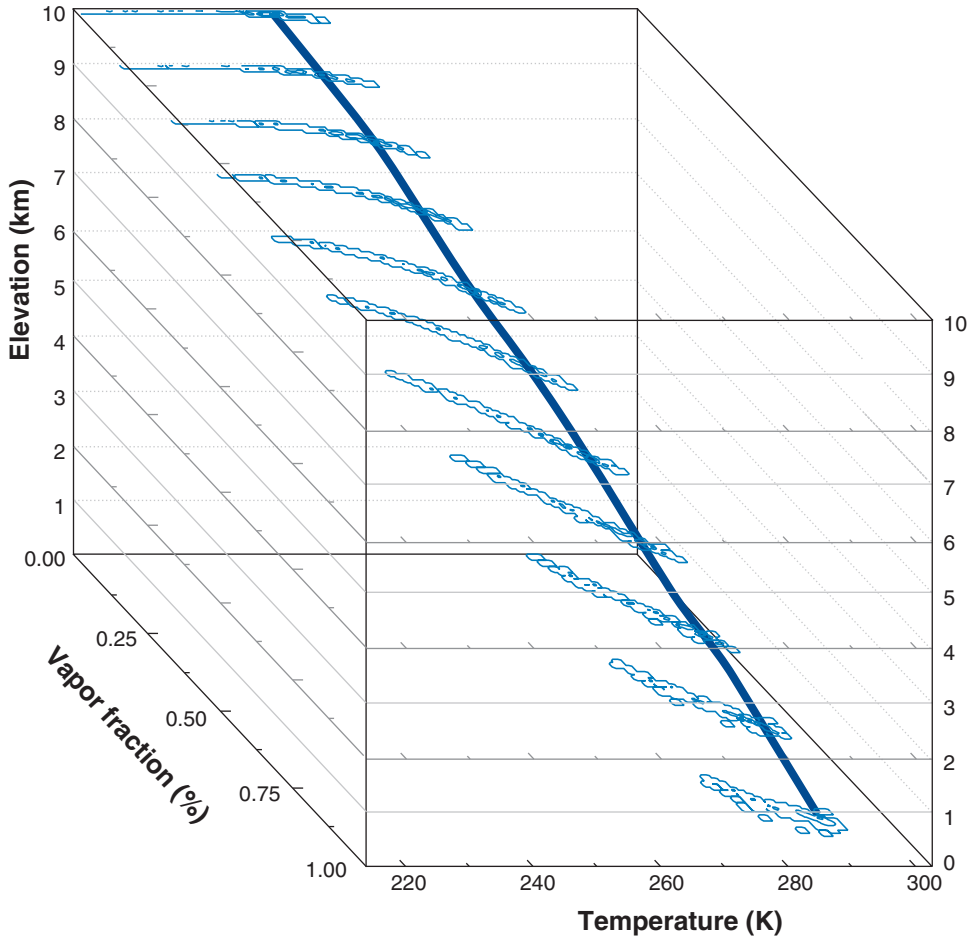

Figure 2

Vertically arrayed probability density function of T and VF of the condensation-weighted mean precipitation falling at each level based on 1000 iterations of the model sampling from the surface T and RH pdf of **Figure 3**. The dark blue line highlights the modal T and VF as a function of elevation. Contour interval is 4%.

it is clear that variations in starting RH result in a relatively small contribution to determining isotopic lapse rate, whereas starting T plays a very significant role. This provides the rationale for the common practice of using $\delta^{18}O$ and $\delta^{2}H$ as proxies for temperature, particularly in ice cores, while recognizing that the real determinant is the ratio of initial water vapor content to water vapor content at the height of the precipitation, and hence the degree of distillation (Pierrehumbert 1999). In addition to providing a quantitative indication of the effect of T and RH on the isotopic lapse rate, **Figure 3** also demonstrates effects of global climate change on the isotopic lapse rate. Obviously, warmer climates yield shallower isotopic lapse rates, whereas colder,

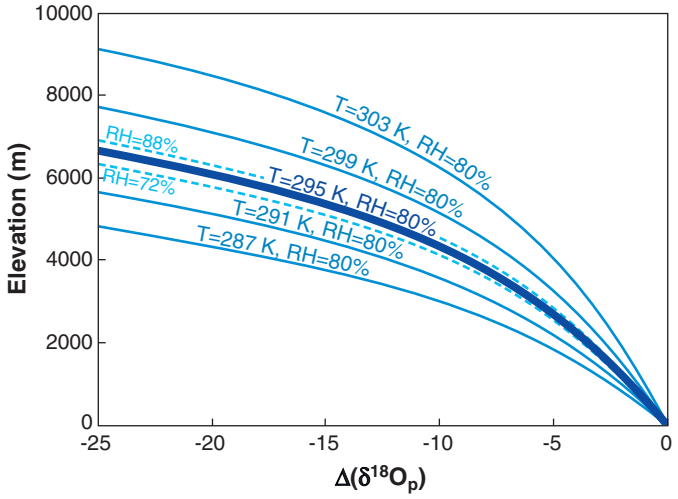

Figure 3

Modeled normalized isotopic composition of precipitation as a function of elevation. Heavy dark blue curve reflects the mean curve derived from the pdf of starting T and RH that corresponds with values of T = 295 K and RH = 80%. Light blue dashed curves reflect the effect of offsetting the starting RH by ±8% while maintaining T at 295 K. Solid light blue curves illustrate the effect of varying starting T by ±4 K and ±8 K while maintaining RH at 80%.

drier climates would be expected to be associated with steeper isotopic lapse rates. On average, much of the geologic past is generally assumed to have been warmer, and hence application of the mean modern lapse rate will underestimate paleoelevations in these cases.

An important question at this point is to what degree does this model capture the relationships that actually exist in nature? In the next section we compare various model predictions relative to observed data from the modern world where there is essentially no uncertainty in either the isotopic composition or the elevations of various samples. The discussion specifically focuses on low-latitude (<35°N or S) examples. There are several reasons for emphasizing this latitude range and not higher latitudes. First, tropical latitudes are more likely to derive moisture from within these latitudes and hence are well represented by the T and RH pdf to estimate isotopic lapse rates. Second, there are strong latitudinal temperature gradients in oceanic source areas at latitudes poleward of approximately 40°, resulting in a significant increase in T variability and hence in estimated isotopic lapse rates at higher latitudes (**Figure 4**). Third, midlatitude and temperate systems are typically characterized by complex frontal systems and air mass mixing with potentially multiple independent moisture sources each with different isotopic, T, and RH characteristics, resulting in much more complex initial starting conditions than are captured in our simple one-dimensional model. We acknowledge that even within ±35°, complex vapor trajectories exist giving rise to complex patterns in the isotopic compositions.

DATA-MODEL COMPARISONS

Critical to the application of this model in paleoaltimetry studies is the assessment of the fit of the model to modern systems for which the first-order isotopic composition as a function of elevation has been determined empirically. As has been well recognized in the isotope precipitation community, the most robust statistic of the

Figure 4

Zonal means for entirely oceanic grid cells in the NCEP reanalysis data (Kalnay et al. 1996) for mean annual T and mean annual RH. Note the increased gradient at higher latitudes, but also the increase in the standard deviation as well.

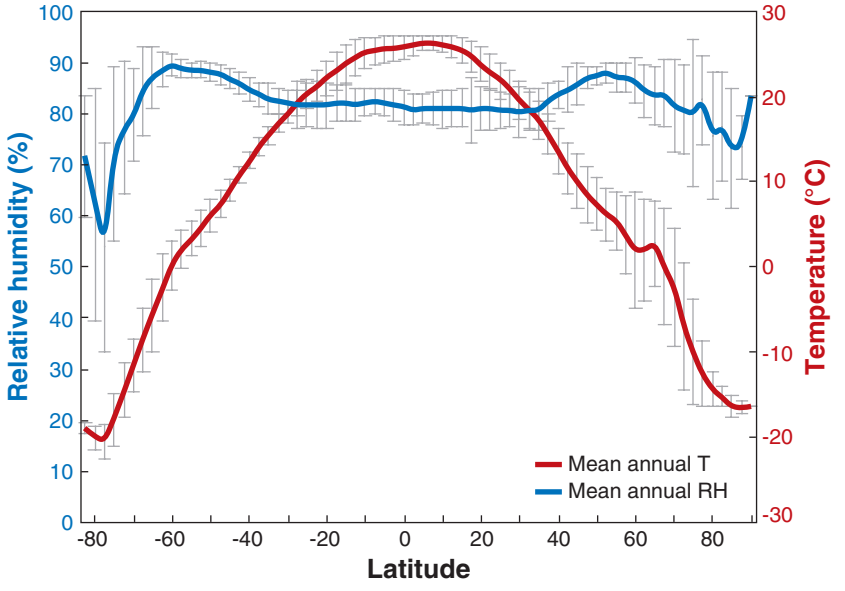

mean isotopic composition at any given station is the precipitation amount-weighted annual mean, where amount is measured in centimeters in a standard rain gauge. This reflects the fact that there is considerable variability in isotopic composition as a function of month or season at most stations, not to mention within single precipitation events. When weighted by how much precipitation falls per month, the amount-weighted mean best captures the actual mean isotopic composition at that station. Similarly, surface waters generally integrate over the mean residence time within the drainage basin and would also be expected to reflect the amounts of precipitation as a function of time rather than just its average isotopic composition. Thus, in the discussion below, we focus entirely on amount-weighted isotopic compositions, unless data on this quantity is not available. The following discussion presents comparisons for modern-day Mount Cameroon, the Bolivian Andes, and Himalaya-Southern Tibet. The latter two have been the primary foci of applications of isotope-based paleoaltimetry research. Data from other systems are discussed but in less detail.

Within a given orographic precipitation regime, relatively few datasets exist that capture long-term estimates of the mean annual isotopic composition of precipitation, weighted for precipitation amount as a function of elevation along simple transects. There are data that allow simple differences to be examined, as done in Rowley et al. (2001), but there are few areas where the functional relationship can be tested explicitly. One exception is the IAEA data from the Alps. However, these data were used to derive the empirical fit between condensation and precipitation (**Supplemental Figure 1**), and hence it would be circular to now use these same data to compare with the model. The best data that we are aware of is from a series of transects that span a large range of elevations reported by Gonfiantini et al. (2001). They reported data from Mount Cameroon and the eastern flank of the Andes in Bolivia.

The transect up Mount Cameroon is based on annual precipitation amount-weighted mean isotopic compositions over 4 years at 25 stations ranging from 10 m to 4050 m elevation. **Figure 5*a*** plots data as $\Delta(\delta^{18}O_p)$ versus elevation, whereas **Figure 5*b*** plots the station elevation against predicted station elevation. In both plots, the standard model curve corresponding with the mean of the low-latitude pdf of T and RH (**Supplemental Figure 2**) is in blue and the isotopic lapse rate associated with a curve based on locally derived climatology for Mount Cameroon (T = 299 K, RH = 80%) is shown in red. It is clear that the model using local climatology does a better job fitting $\Delta(\delta^{18}O_p)$ than does the global mean model, but both models provide reasonable fits, with a mean deviation of 150 m using the local climatology and 461 m using the global model for stations above 1000 m (**Figure 5*b***). All of the measured compositions plot within $\pm 2\sigma$ of the global mean lapse rate curve.

Gonfiantini et al. (2001) also provide shorter-term data from the Bolivian Andes. **Figure 6** shows the relationship between predicted station elevation and station elevation for stations along the transect from Trinidad through Sapecho to El Alto based on the global model. The data are derived from table 6 of Gonfiantini et al. (2001) with weighted values normalized to the weighted mean of Trinidad (−5.2‰) and unweighted data to the unweighted mean of Trinidad (−3.84‰).

The good fit of the Mount Cameroon and Bolivian Andes isotopic data of Gonfiantini et al. (2001), with predictions based on modeled thermodynamics and the empirically derived scheme for converting condensation into precipitation, suggests that the model captures the first-order controls on the isotopic composition of precipitation with elevation. Cloud microphysics, including raindrop size distributions and evaporation and large-scale turbulent mixing that are not explicitly part of the existing model appear to play relatively minor roles in establishing the isotopic lapse rate in precipitation in these low-latitude climate regimes. Of course the empirical fit to the observational data on isotopic composition in the Alps may incorporate aspects of these effects to the extent that they are present in the Alpine data. The absence of significant additional contributions is quite fortunate, as it is difficult to factor these into paleoaltimetry estimates where an independent ground truth is not possible to establish. An important aspect of this work is that, at least at higher elevations, predicted elevations tend to be close to known elevations, and where they differ there is a tendency for the model to underestimate rather than overestimate elevations. We return to this topic below after we discuss other modern datasets, and particularly various surface water samples.

SURFACE WATERS

Virtually all archives that might be used for paleoaltimetry purposes derive their isotopic signatures from either surface or ground waters. Surface waters in particular, and ground waters to a lesser degree, differ in important ways from precipitation. Before examining modern surface waters, and specifically river and stream water isotopic compositions as a function of elevation, we need to discuss the nature of those differences.

The most important difference between surface or ground waters and precipitation is that rivers and streams integrate precipitation in the drainage basins above the point that a sample is taken. Ramesh & Sarin (1995) concluded that the mean elevation of the drainage basin above the sample elevation should be recorded by the isotopic composition of stream or river waters. They pointed out that by assuming a constant precipitation amount as a function of elevation, the isotopic lapse rate in

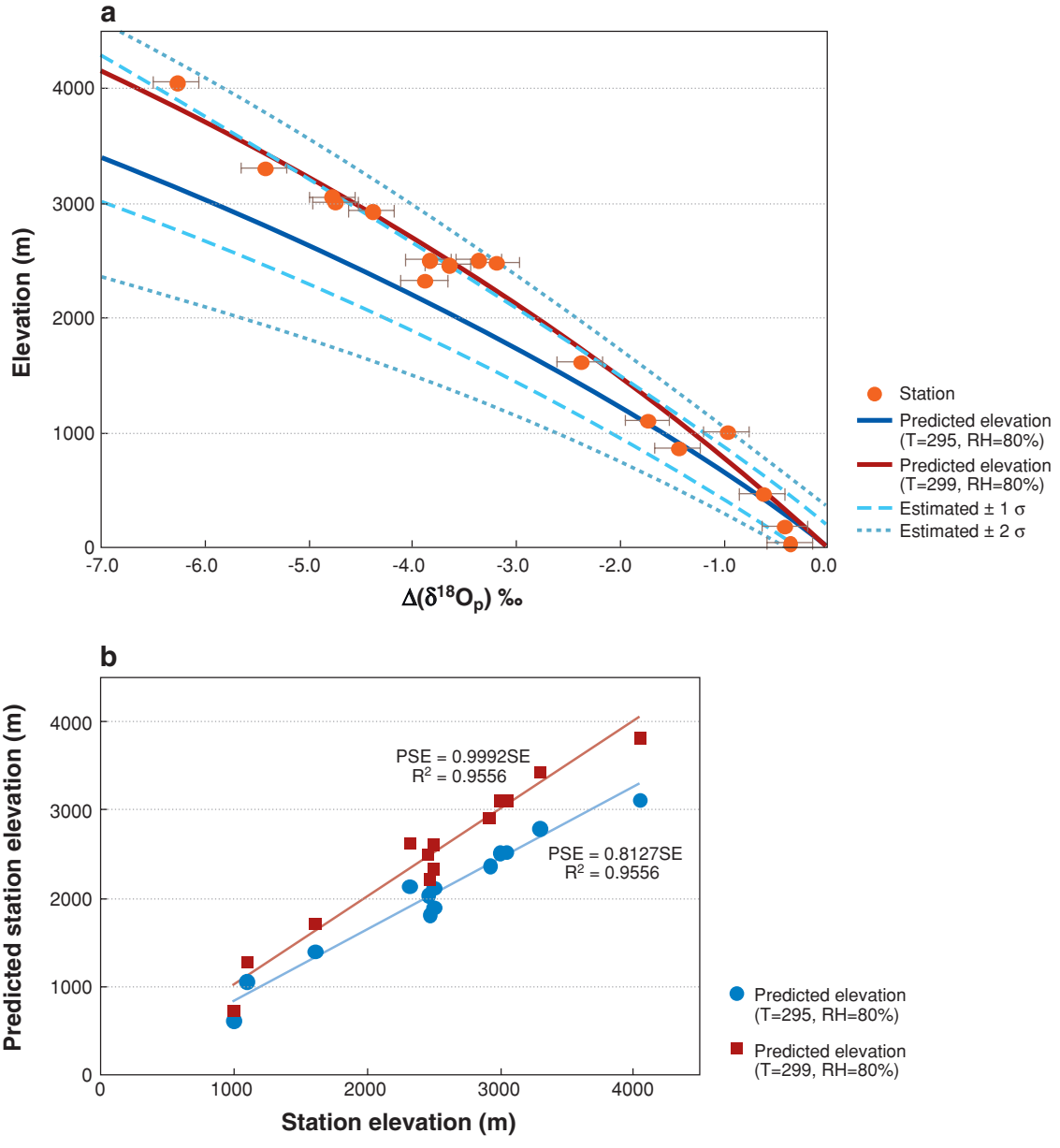

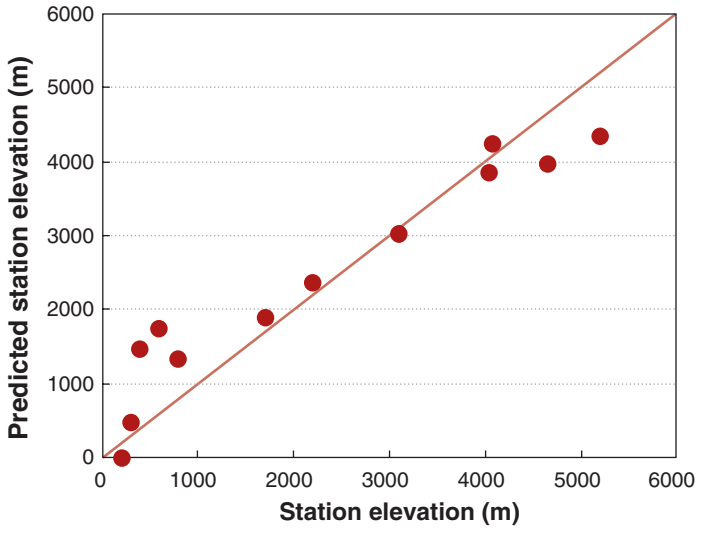

Figure 6

Bolivian Andes transect from Trinidad (200 m) through Sapecho to El Alto (4080 m) from Gonfiantini et al. (2001). Predicted station elevation based on normalization relative to Trinidad using modeled global mean isotopic composition as a function of elevation.

streams should be about half that in the source precipitation. However, the Ramesh & Sarin (1995) approach ignored the effects of basin hypsometry on the integration of precipitation above the sample site and the fact that precipitation amount varies as function of elevation (see below). Hypsometry in drainage systems is not a simple linear function of elevation and hence cannot be simply represented by the average of the maximum and sample elevation as assumed by Ramesh & Sarin (1995). Rather, the hypsometry of each drainage system needs to be computed individually. One consequence of this hypsometric effect is that isotopic compositions along rivers and streams should not be expected to vary in a simple linear fashion with elevation. This is nicely demonstrated in the compilation of Poage & Chamberlain (2001).

Precipitation amount also varies as a function of elevation, sometimes with strong gradients in orographic systems, particularly at relatively low elevations (<3–4 km) (Burbank et al. 2003, Putkonen 2004). Anders et al. (2006) and Roe (2005) have

Figure 5

(*a*) Mount Cameroon $\Delta(\delta^{18}O_p)$ versus elevation based on amount-weighted mean compositions of precipitation as a function of elevation reported by Gonfiantini et al. (2001) for each station. Dots are measured differences in isotopic composition relative to the amount-weighted mean isotopic composition ($-3.2 \pm 0.2‰$) of the four low-elevation (<100 m) stations. Blue curve is the standard model. Red curve shows predicted isotopic lapse rate corresponding with the climatologic average observed at the low elevation stations. Long dashed curves are estimated $\pm 1\sigma$ and short dashed curves are $\pm 2\sigma$ deviations based on Monte Carlo simulations. (*b*) Mount Cameroon station elevation (SE) versus predicted station elevation (PSE) based on amount weighted mean compositions of precipitation as a function of elevation reported by Gonfiantini et al. (2001) for each station. Predictions based on fits of curves to model results for starting conditions corresponding with the global mean T and RH data (*blue*) and local low-elevation mean climatology (*red*). Regression lines through the origin and correlation are shown for each.

provided a large-scale mapping of precipitation rate as a function of orography in the Himalaya and Tibet region using the Tropical Rainfall Measurement Mission (TRMM) satellite data. They modeled the precipitation as a function of elevation and as a combination of the change in saturation vapor pressure as a function of temperature (and hence elevation) and surface slope (Anders et al. 2006, Roe et al. 2002). We use their data to examine, in the regional sense of the Himalayas, the relationship between elevation and precipitation amount. To specifically focus on orographic precipitation in the Himalayas, a subset of the Anders et al. (2006) data was extracted that lies within a 300-km-wide swath north of the Himalayan front. Our purpose is not to predict the spatial variability of precipitation as a function of elevation, as has been done by Anders et al. (2006), but rather to look for the most general pattern so as to allow a better understanding of the information content of measurements of the isotopic composition of surface waters.

Figure 7 demonstrates that both the weighted mean precipitation and median precipitation above about 1000 m show a simple linear decrease in precipitation

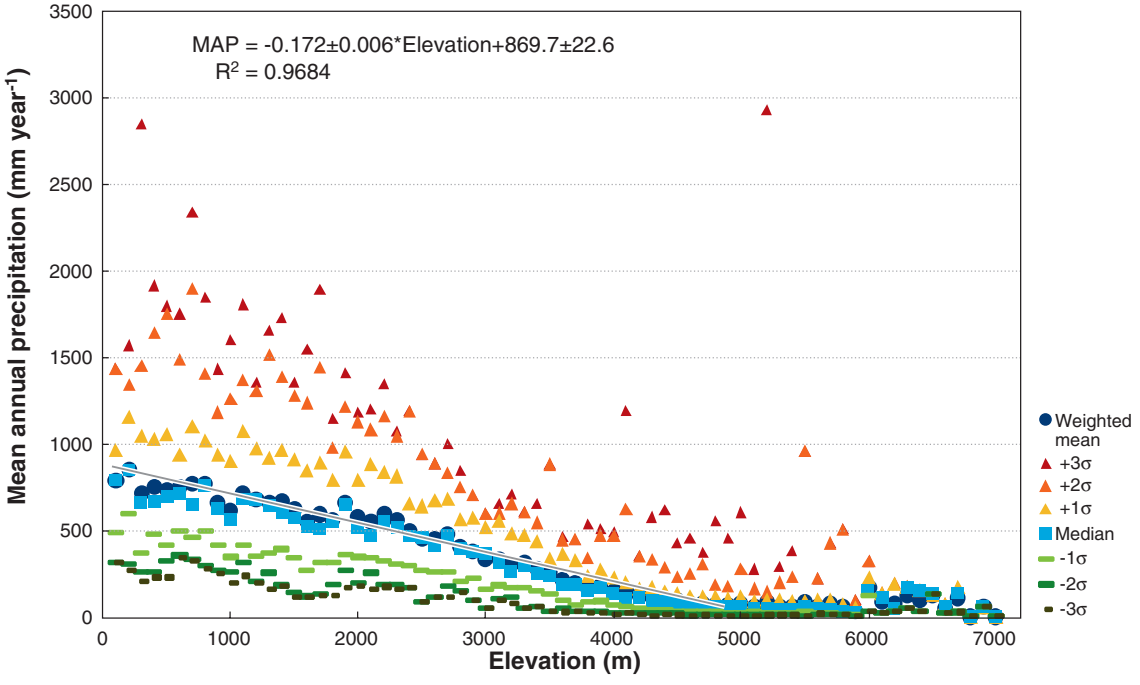

Figure 7

TRMM-based estimates of mean annual precipitation as a function of elevation based on data from Anders et al. (2006). The regression analysis is of precipitation versus elevation from the front to 4600 m elevation in the 300-km-wide swath north of the Himalayan Front from 73.55°E to 95.55°E longitude. For our purposes, the Himalayan front is defined as coinciding with about the 200 m contour, except west of 80°E, where it rises slightly in the region of the divide between the Indus and Ganges drainages. Data from north and south of this 300-km-wide swath are excluded from this analysis.

amount with increasing elevation. Anders et al. (2006) demonstrate that this relationship accords with a dominant correlation to the rate of condensation as a function of temperature (and hence elevation). This linear relationship appears to be largely controlled by the shape of the water saturation vapor pressure curve, the derivative of which is linear with respect to temperature (Roe et al. 2002, Anders et al. 2006). The plot shows that the average amount of precipitation decreases linearly with elevation from the Himalayan Front to about 4600 m, above which precipitation amount is approximately constant at about 74 mm/year. The graph also shows $\pm 1\sigma$, $\pm 2\sigma$, and $\pm 3\sigma$ variations of the TRMM estimates of precipitation amount around the median, as estimated from the data within this swath. Each of these also clearly shows the decreasing trend with elevation, but indicates that significant variability exists. Again, for our purposes, we emphasize that precipitation amount varies as a function of elevation, and as discussed below, this has a significant impact on the interpretation of the stable isotopic compositions of surface waters, particularly of low-elevation samples in the forelands of mountains.

From the above discussion, surface water isotopic compositions should reflect the hypsometry of the drainage basin above the sampling site integrated with the amount of precipitation falling as a function of elevation on that hypsometry. Thus, the isotopic composition of a river or stream sample should reflect the precipitation amount-weighted hypsometric mean elevation of the drainage basin above the elevation at which a sample was taken. We compare surface water isotopic compositions with various measures of the hypsometry. For the Himalayas, we model isotopic compositions using both the spatial distribution of precipitation, assuming that the four year interval sampled by Anders et al. (2006) is representative and by applying the regression analysis (**Figure 7**) to estimate the precipitation amount on the drainage basin hypsometry. In other cases, the parameter derived directly from the model that most closely matches the precipitation amount-weighted hypsometric mean elevation is provided by the condensation-weighted hypsometric mean elevation where the predicted isotopic composition is weighted by the variation in amount of condensation in the air parcel above each elevation bin of the hypsometry.

One important consequence of this hypsometric effect is that isotopic compositions along rivers and streams should not be expected to vary in a simple linear fashion, nor, as pointed out by Ramesh & Sarin (1995), should the isotopic lapse rate of precipitation and the isotopic lapse rate determined from surface waters be the same [as assumed by Chamberlain & Poage (2000)].

Quite extensive data sets exist for Himalaya–Southern Tibet. Below we summarize our findings derived from analysis of a small subset of these data in the context of the model presented above. Note that this approach is different from that adopted by Garzione et al. (2000a,b) who derived the isotopic lapse rate by empirically fitting a curve to observed surface water data. We show that given a known starting composition, both approaches produce approximately the same results within the present uncertainty of the technique, but that understanding the underlying climatic controls on the isotopic lapse rate allows an understanding of potential effects of climate change to be factored into the analysis. Here we use the model to predict the mean elevation of rainfall in the drainage basin weighted by the amount of precipitation.

Garzione et al. (2000a,b) sampled stream waters ascending the south-facing flank of the Himalayas in small tributaries draining into the Seti and Kali Gandaki rivers. **Figure 8*a*** plots these data in terms of $\Delta(\delta^{18}O_{mw})$, against precipitation falling in New Delhi (−5.81‰ ± 1.8, IAEA 1992), which provide low-altitude normalization. Estimates of the elevation range of each drainage (Garzione et al. 2000b) are plotted, as is the predicted elevation based on the isotopic composition in terms of $\Delta(\delta^{18}O_{mw})$ of each of the samples. Perhaps a visually better way to examine these data is to

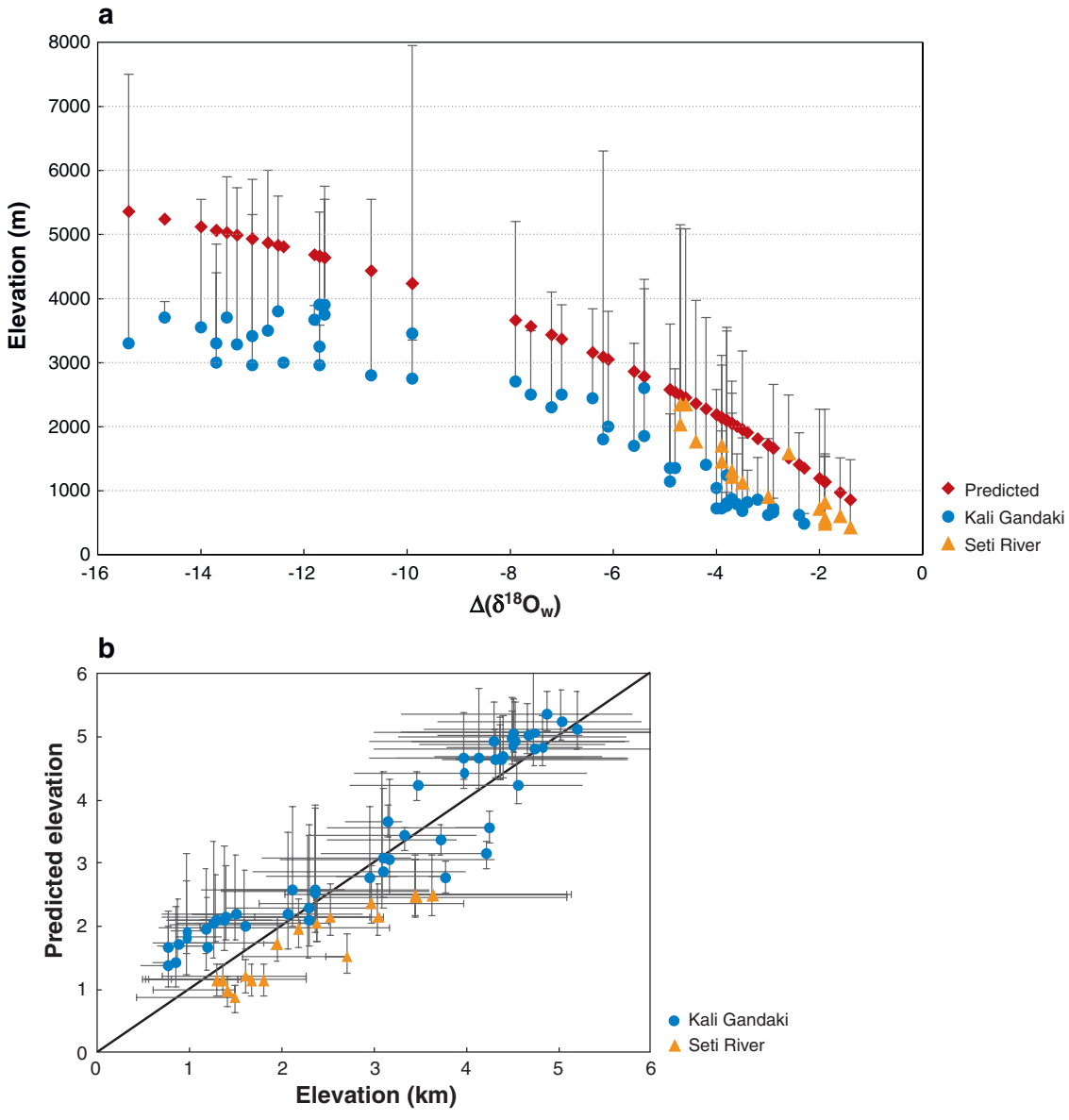

plot the sample-related elevations, specifically the sample elevation, precipitation-weighted hypsometric mean elevation, and maximum elevation along the x-axis and the elevation predicted from the sample isotopic compositions and their uncertainty on the y-axis (**Figure 8*b***). The data clearly plot close to the 1:1 line of correlation and overlap the line within uncertainty, demonstrating that the model captures significant aspects of the relationship between isotopic composition and elevation in this region.

Intermontane basins provide the best archive in modern orographic settings within which to determine paleoaltitude histories. However, in deeper time the prevalence of preserved foreland basins make these potentially attractive sites for estimating the former heights of adjacent mountains. This raises the important issue in the paleoaltimetry of mountains and plateaus as to whether it is possible to discern the heights of adjacent mountains from measurements of the isotopic compositions of proxies within foreland basin sedimentary sections. The existence of a foreland basin implies flexural loading, and hence topography; but is it possible to discern how high the adjacent mountains are based on isotopic compositions measured in proxies preserved within such sediments, particularly within preserved fluvial channels? Thus is it possible to measure, for example, the isotopic compositions of bivalve shells or fish, reptilian, or aquatic mammalian teeth preserved within such sediments to determine how high the adjacent mountains were? We address this question using modern river isotopic compositions from the Himalaya region, and particularly from the Ganges drainage (**Figure 9*a***) based on data from the Ramesh & Sarin (1995) summary of isotopic compositions from various rivers in the Ganges and Brahmaputra drainages.

The most important aspect of **Figure 9*b*** is yet another demonstration that the model captures significant information regarding the elevation distribution contributing to each of the drainage basins derived from the Himalayas. There is a close correspondence between the predicted elevations and the precipitation-weighted hypsometric mean elevation of the drainage above the sample site as well as the

Figure 8

(*a*) Isotopic composition as $\Delta(\delta^{18}O_{mw})$ versus elevation diagram for samples of small drainages sampled within the larger Kali Gandaki (*blue dots*) and Seti River (*orange triangles*) drainages. The vertical lines represent the height of the drainages sampled by these streams above the collection site. Red diamonds represent the predicted elevations corresponding with the isotopic composition of each of the samples. Note that virtually all of the predicted elevations (*diamonds*) lie within the range of each of the drainages, and hence these data are compatible with model predictions. Note also that Garzione et al. (2000a) used linear regression through the Seti data of $\delta^{18}O_{mw}$ versus elevation to establish the lapse rate and associated estimate of paleoelevation of the Thakkhola graben. Garzione et al. (2000b) used a polynomial fit to the Kali Gandaki data of $\delta^{18}O_{mw}$ versus elevation to estimate paleoelevations of the Thakkhola graben. (*b*) Precipitation-weighted hypsometric mean elevation versus elevation predicted from $\Delta(\delta^{18}O_w)$ with associated 1σ uncertainty of each of the samples from the Kali Gandaki (*blue dots*) and Seti River (*orange triangles*) drainages reported by Garzione et al. (2000a,b). Horizontal bars represent the sample elevation and maximum elevation in the drainage basin. Solid line is the 1:1 line of correlation. The mean deviation of individual estimates from the predicted elevation is 487 m.

simple hypsometric mean elevation of the drainage basin above the sample elevation. What would one infer about the elevation of the Himalayas from these isotopic compositions? The answer is pretty clear: the precipitation-weighted hypsometric mean elevation of the drainages. However, it would be extremely difficult to surmise the existence of high Himalayan peaks rising above 7000 m to 8000 m, 4 to 6 km

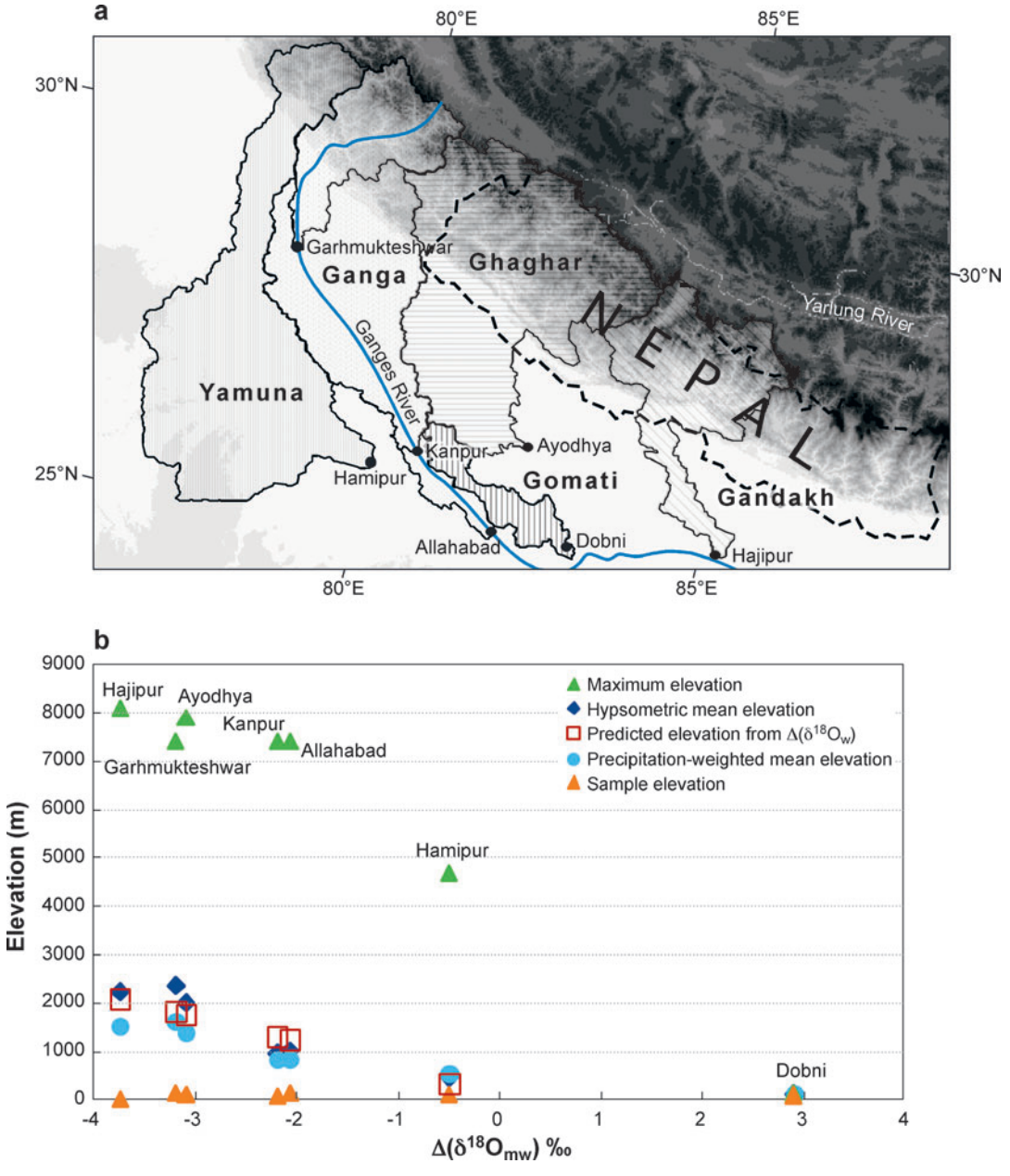

above the hypsometric mean elevations. It would also be impossible to differentiate between the real situation and a plateau region, with a mean elevation just above the hyposometric mean. These would represent significantly different topographies with significantly different tectonic implications. This cautions against approaches that utilize low-elevation, fluvially derived, foreland basin estimates of the heights of adjacent mountains. A signal exists, as is clear from **Figure 9*b***, but the interpretation requires considerable care, particularly in choosing corresponding low-elevation data to normalize the isotopic composition and in recognizing both the hypsometric and elevation dependence of the precipitation amount effects on the measured isotopic compositions. These effects are considerably reduced when data are collected in intermontane basins at relatively high elevation, as has been the approach of Rowley et al. (2001), Currie et al. (2005), Rowley & Currie (2006), Garzione et al. (2000a,b; 2006), and Ghosh et al. (2006b).

Carbonate Records of Paleoelevation

Paleoaltimetry requires an archive that has the potential of preserving the $\delta^{18}O$ or $\delta^{2}H$ of the water from which the sampled material derived its isotopic composition. The archive of stable isotopic compositions preserved in the geologic record is virtually entirely sampling some aspect of surface waters or groundwater-derived isotopes and not precipitation directly. Therefore samples have the potential to reflect effects associated both with surface or subsurface transport and with evaporation that will effect their composition relative to precipitation falling at a particular elevation. Effects associated with evaporation leave a distinctive isotopic signature in the remaining water characterized by ^{18}O enrichment relative to ^{2}H when plotted against the GMWL. Evaporation will always lead to heavy isotope enrichment and an underestimation of paleoelevation.

Sedimentary carbonates are precipitated from surface waters from various sources. Paleosol carbonates likely reflect rainfall that infiltrated the soil during the season of

Figure 9

(*a*) Drainage basins above sample locations of riverine oxygen isotopic measurements reported by Ramesh & Sarin (1995). Sample sites are in cities marked by black dots. The drainage basin outlines and basin statistics are based on analyses of the Hydro1K elevation data. (*b*) Elevation versus $\Delta(\delta^{18}O_{mw})$, where the isotopic composition of precipitation in New Delhi is used to normalize compositions. Isotopic data reported by Ramesh & Sarin (1995) include both oxygen and/or hydrogen isotopic compositions. Hydrogen isotopic compositions were converted to oxygen isotopic compositions using $\delta^{18}O = (\delta^{2}H\text{-}10)/8$. Note that the precipitation-weighted mean elevations use actual precipitation amounts estimated from TRMM by Anders et al. (2006) and topography regridded at the same tenth-of-a-degree resolution and spatial locations as the precipitation data. This significantly smoothes topography relative to the 1 km resolution of the Hydro1K and an average difference of about 100 m in estimates of the hypsometric mean elevations within each drainage basin derived from these different digital elevation models (DEM). Where data are available from more than a single sample the average composition is used. Predicted elevations based on $\Delta(\delta^{18}O_{mw})$ using Equation 1 from Currie et al. (2005).

carbonate precipitation. Lake carbonates precipitate from river water and groundwater that are sourced from surrounding drainage basins and thus convolve hypsometric and elevation-dependent precipitation amount effects with potential evaporation effects. Therefore, paleosol carbonates are likely to be better proxies for local rainfall composition.

It is important to remember that given typical sedimentation rates of micritic carbonate in lacustrine settings and soil carbonate accumulation rates, individual samples integrate thousands to perhaps tens of thousands of years. This means that such samples are recording millennial signals at best, and hence represent a very smoothed record relative to the high-frequency signals preserved in typical ice core records. For paleoaltimetry purposes, this represents a positive bias in that we are seeking long-term means and not short-term variability in which climate change signals play a potentially important role.

In carbonate studies, fractionation of oxygen isotopes is associated with the temperature of carbonate precipitation, with $\sim -1‰$ per 5°C (Friedman & ONeil 1977, Kim & O'Neil 1997). This fractionation is much smaller than the Rayleigh distillation-related fractionation associated with changes in elevation. However, because paleoelevation is the unknown, calculations that assume a paleotemperature for water during carbonate deposition, which in part depends on altitude, introduce significant uncertainty. In some regions, mean annual paleotemperature constrained from leaf physiognomy data can be used for available time periods to minimize the error associated with this uncertainty. Mean annual temperatures estimated from paleoleaf data (e.g., Wolfe 1993) generally have a 1σ uncertainty of ± 2 to 3°C (Gregory-Wodzicki et al. 1998, Forest et al. 1999). These temperature estimates yield information about surface conditions, but not necessarily the temperature of carbonate formation because carbonates tend to form preferentially during certain seasons. For example, paleosol carbonates may form during the dry season when evaporation rates are highest (Liu et al. 1996) and/or during the growing season when evapotranspiration rates are highest (Cerling & Wang 1996). Mean annual temperature estimates along with modern seasonal temperature variations can be used to gauge the average temperature during the season of paleosol formation. Because paleosol carbonates usually form close to the surface ($\sim$1 m or less), they probably reflect mean atmospheric temperatures during the season of carbonate formation.

Lacustrine carbonate, typically micritic limestones, referred to below simply as micrites, tends to become supersaturated during the summer when evaporation rates are highest and carbonate has the lowest solubility, leading to whiting events (widespread formation of microcrystalline carbonate) during discrete intervals when the lake water is warm (e.g., Duston et al. 1986, Effler & Johnson 1987). Because micrite forms during the same season and under similar conditions each year, temperatures during other seasons do not have a large effect on the $\delta^{18}O$ of lacustrine carbonate (McKenzie 1985, McKenzie & Hollander 1993, Drummond et al. 1995, Hodell et al. 1998). Organisms, such as mollusks, that precipitate aragonite shell material do so within a specific range of water temperatures. The temperature of shell precipitation of ancient organisms that have modern relatives can be estimated and applied to fossil material (Dettman et al. 1999, Dettman & Lohmann 2000).

Even with knowledge of the season of carbonate formation in both paleosol and lacustrine carbonate records, we still have to assume seasonal temperatures that are in part controlled by the elevation of the depositional basin. A new carbonate thermometer based on the clumping of ^{13}C and ^{18}O with each other in the carbonate mineral lattice (Ghosh et al. 2006a) may help mitigate this uncertainty in future studies (see discussion below).

Diagenesis can also alter the $\delta^{18}O_c$ value of carbonate, depending on the temperature of calcitization or recrystallization and/or the source of fluids involved in the diagenesis. Calcitization will not modify the $\delta^{18}O_c$ value if it occurs at temperatures similar to surface temperatures and in equilibrium with the original pore fluids in the carbonate. This is typically the case for diagenesis early in the history of carbonate deposition. However, higher temperature recrystallization (>40°C) or recrystallization/calcitization in the presence of later fluids moving through the rocks can modify the original $\delta^{18}O_c$, rendering these carbonates useless in studies of paleoelevation (Morrill & Koch 2002; Garzione et al. 2004). It is therefore important to evaluate the history of diagenesis both petrographically and isotopically to determine the relative timing of diagenetic events, the isotopic composition of different diagenetic phases, and their formation temperature.

Uncertainty

Large uncertainties are inherent in modeling the isotopic evolution of water vapor and the rainfall derived from it (see above). Having shown that the model provides a good fit to empirical observations of the isotopic evolution of rainfall and surface waters, the best way to constrain the errors associated with paleoelevation estimates in settings where climate/paleoclimate is reasonably well understood is to propagate the uncertainties observed in empirical data and use the model to understand potentially significant additional contributions from climate change, particularly associated with changes in temperature. These other uncertainties include (*a*) scatter in the data that define the $\delta^{18}O_{mw}$ versus altitude relationship if one is employing an empirical approach and (*b*) uncertainties associated with converting the $\delta^{18}O_c$ to values of $\delta^{18}O_{mw}$.

Scatter in data that define the relationship between $\delta^{18}O_{mw}$ and altitude is observed in rainfall data or surface water data that have been systematically sampled along an elevation transect that reflects the transport pathway for water vapor. For example, the scatter in unweighted[1] mean isotopic composition of rainfall sampled across the eastern mountain front in Bolivia (Gonfiantini et al. 2001) can be used to propagate uncertainties for elevation estimated in the Andes, whereas scatter in the isotopic composition of small tributaries sampled within the Kali Gandaki drainage on the southern flank of the Himalayas (Garzione et al. 2000b) is used for the Himalayas and southern Tibet. Alternatively, as shown in the analyses of model versus modern precipitation and surface water samples, estimated uncertainties from the model,

[1]Table 5 from Gonfiantini et al. (2001), which is the source of data for the analysis reported by Garzione et al. (2006), mislabels the columns such that reported weighted means are actually unweighted means.

primarily reflecting the spectrum of potential starting T and to a lesser degree RH, typically represent quite reasonable bounds on the estimates of (paleo)elevation. One of the critical problems in using existing empirical datasets is that they typically sample very short intervals of time relative to the millennial timescales averaged by geological samples, and hence it is difficult to assess how representative they are of the actual long-term mean state of the system. Only high elevation ice cores in the Andes (Thompson 2000) and Himalayas and Tibet (Thompson et al. 1989), among other sites, provide potentially statistically meaningful samples of isotopic variability induced by climate variability at specific elevations but not along an elevation transect. This probably results in the empirical samples underestimating the variance of isotopic compositions when empirical calibrations are employed.

Uncertainties associated with converting the $\delta^{18}O_c$ to the corresponding $\delta^{18}O_{mw}$ derive from both (*a*) uncertainties in the empirical temperature-dependent fractionation equation between water and carbonate (Kim & O'Neil 1997) and (*b*) uncertainty in the assumed temperature of carbonate precipitation. Kim & O'Neil (1997) developed a number of empirical relations for the temperature dependence of the fractionation factor in a variety of minerals. The empirical relation ($R^2 = 0.997$), with standard errors, is reported as a linear fit to natural log normalized data:

$$1000 \ln \alpha_{ew} = 18.03 \pm 0.36(1000T^{-1}) - 32.42 \pm 1.22, \quad (5)$$

where T is temperature of water in Kelvin and the fractionation factor $\alpha_{c-w} = (\delta^{18}O_c + 1000)/(\delta^{18}O_w + 1000)$. The uncertainty in the slope and intercept are based on analysis of the data presented by Kim and O'Neil (1997). Although the uncertainty in this empirical fit is small, it is incorporated into the error propagation. A much larger source of error in paleoelevation estimates arises from assuming a temperature for carbonate precipitation in Equation 5 to calculate $\delta^{18}O_{mw}$ value. This uncertainty (~100 to 300 m) can possibly be reduced by applying a new calcite paleothermometer that determines growth temperature from the abundance of ^{13}C–^{18}O bonds in the calcite mineral lattice (Ghosh et al. 2006a,b). Determining the mean temperature and standard deviation from a suite of samples from the same time period can reduce the temperature uncertainty to $< \pm 3^\circ C$ (Ghosh et al. 2006b).

In regions where the paleoclimate is fairly well understood, the uncertainty in elevation estimates can be propagated using a bootstrap approach that includes the errors described above together with uncertainties in the isotopic composition of low-elevation precipitation used to determine $\Delta(\delta^{18}O_{mw})$. A bootstrap approach is preferable to geometric estimation of uncertainty because significant covariance exists between the $\delta^{18}O$ value of meteoric water, T, and elevation. In both the Andes and the Himalayas/Tibet, bootstrap simulations, assuming uncertainty in the temperature of carbonate precipitation of $\pm 5^\circ C$, produce 1σ errors of ± 1000 m at paleoelevations of less than 500 m that decrease to ± 400 to ± 500 at elevations more than 4 km. The greater uncertainty at lower elevation results from several factors, including the lower isotopic lapse rate of $\delta^{18}O$ and the greater degree of scatter in rainfall and surface water data at low altitude reflecting nonorographic effects.

Additional systematic errors cannot be propagated. These errors include (*a*) climate and paleogeographic changes that may have led to a change in the source of

moisture and/or the $\delta^{18}O$ versus altitude relationship and (*b*) evaporation of surface waters from which carbonates precipitated. The first systematic error can be mitigated to some degree through understanding the climate history of the region and documenting a low altitude site that records the isotopic composition of the source moisture. For instance, the Siwalik Group, deposited in the foreland basin south of the Himalayas, provides a record of both climate (e.g., Quade et al. 1989, 1995; Dettman et al. 2001; Hoorn et al. 2000; Nelson 2005) and the isotopic composition of low-elevation precipitation (Garzione et al. 2000b, Rowley et al. 2001, Currie et al. 2005). The second source of systemic error results from evaporation of surface waters from which carbonates precipitated. Evaporation produces enrichment in ^{18}O, which results in an underestimation of paleoelevation. This underestimation of elevation is witnessed in several modern Himalayan lakes (Rowley et al. 2001) and has been documented in several paleoelevation studies comparing paleosol carbonates with lacustrine and palustrine (pond/marsh) deposits (Currie et al. 2005, Garzione et al. 2006). In both cases, lacustrine carbonates showed significant evaporative enrichment in ^{18}O relative to paleosol carbonates, which limited their use in estimating paleoelevation. One approach followed by Cyr et al. (2005, and references therein) is to examine the major cation chemistry (e.g., Mg/Ca or Sr/Ca) of lacustrine carbonates in comparison with $\delta^{13}C_c$ and $\delta^{18}O_c$ to determine whether covariations expected from evaporative enrichment exist. Although paleosol carbonates appear to provide a better record of elevation, they are also prone to varying degrees of evaporative enrichment in soil water (Cerling & Quade 1993, Liu et al. 1996). Because surface water evaporation always produces an underestimation of elevation, this suggests that the most negative $\delta^{18}O$ values of carbonates (highest elevation estimates) provide the best record of elevation.

New Directions in Carbonate Stable-Isotope Paleoaltimetry

A new carbonate paleothermometer relies on the abundance of ^{13}C–^{18}O bonds in the calcite mineral lattice (Ghosh et al. 2006a). This paleothermometer can be used in studies of paleoelevation in several ways: (*a*) The growth temperatures of surficial carbonate can be compared to the measured T lapse rate over land to determine paleoelevation; (*b*) the growth temperature of carbonate more precisely constrains the $\delta^{18}O_{mw}$ from which the carbonate grew (because both the growth temperature and $\delta^{18}O$ of carbonate are known), which can be compared with the altitude dependence of the $\delta^{18}O$ of meteoric water (Garzione et al. 2006); (*c*) independent constraints on the carbonate growth temperature and isotopic composition of water from which carbonates precipitated enable the comparison of these two variables to the mean annual surface temperature and the annual weighted average $\delta^{18}O_{mw}$ across an elevation transect to calculate elevation (Ghosh et al. 2006b).

Δ_{47} Paleothermometry. Molecules of CO_2 containing more than one rare isotope (multiply substituted isotopologues) have low natural abundances at the parts-per-million to parts-per-billion level by fraction (Eiler & Schauble 2004). Despite this

low abundance, precise measurements of the abundance of multiply substituted isotopologues have been made below the 0.1‰ level in atmospheric gases and synthetic carbonates (Eiler & Schauble 2004, Ghosh et al. 2006a). The most common multiply substituted molecule of CO_2 is $^{18}O^{13}C^{16}O$, with a mass of 47 atomic mass units. This isotopologue is ten to one thousand times more abundant than other multiply substituted molecules, and it is therefore the easiest to measure with high precision (Eiler & Schauble 2004). The abundance of mass 47 is measured relative to mass 44 ($^{16}O^{12}C^{16}O$) to yield a ratio, R^{47}, of which 97% is $^{18}O^{13}C^{16}O$ (the remaining 3% consists of $^{18}O^{12}C^{17}O$ and $^{17}O^{13}C^{17}O$). The measured R^{47} is reported as Δ_{47} in per mil, which is referenced to the R^{47}_{random} predicted from the random distribution of heavy isotopes in the same sample. R^{47}_{random} is calculated from the measured $\delta^{13}C$ and $\delta^{18}O$ values of each sample (Eiler & Schauble 2004). The Δ_{47} value is defined as

$$\Delta_{47} = \left(R^{47}_{measured}/R^{47}_{random} - 1\right) \cdot 1000. \quad (6)$$

It has long been recognized that multiply substituted molecules have different thermodynamic properties from singly substituted molecules (containing one rare isotope) (Bigeleisen & Mayer 1947, Urey 1947). Molecules that contain two heavy isotopes have lower zero point energies than normal or singly substituted molecules (Urey 1947, Bigeleisen & Mayer 1947, Wang et al. 2004), which means that they form stronger bonds than their light isotope counterparts. As temperature increases, increasing vibrational energies tends to break heavy isotope and light isotope bonds more equally than at lower temperature. Therefore, in an equilibrium reaction, the abundance of multiply substituted molecules increases at lower temperatures (Wang et al. 2004). Carbonates that form at the surface of the Earth precipitate from water in a range of temperatures sensitive to multiply substituted heavy isotopes in CO_3. The abundance of $^{18}O^{13}C^{16}O$ in CO_2 produced by phosphoric acid digestion has been shown to be proportional to the abundance of $^{18}O^{13}C^{16}O_2^{2-}$ in carbonate, enabling the calibration of a carbonate paleothermometer using synthetic calcites that were precipitated over a range of temperatures representative of surface environments (Ghosh et al. 2006a). The calibration is well fit by a linear relationship of

$$\Delta_{47} = 0.0592 \cdot 10^6 \cdot T^{-2} - 0.02, \quad (7)$$

which is applicable to carbonates that precipitated over a temperature range of 1°C to 50°C (Ghosh et al. 2006a), with T in Kelvin.

The application of this carbonate paleothermometer may be especially useful in paleoelevation studies in arid environments where standard oxygen isotope techniques cannot be applied owing to evaporative reenrichment of surface waters or precipitation as it falls into highly undersaturated air. Rather than using changes in $\delta^{18}O$ with altitude to quantify elevation, the growth temperatures of surficial carbonate can be compared to the measured T lapse rate over land to determine paleoelevation, acknowledging that lapse rates of T are sensitive to climate change as are lapse rates of stable isotopes.

The uncertainty in standard stable isotope paleoaltimetry, aimed at using the estimated $\delta^{18}O$ value of surface water to calculate paleoelevation, is large (1σ of 400 to

1000 m) partly due to uncertainty in the carbonate growth temperature. Determining the growth temperature of carbonate more precisely constrains the $\delta^{18}O$ of water from which carbonate grew because both the growth temperature and $\delta^{18}O$ of carbonate are known. In the standard oxygen isotope paleoaltimetry approach, this reduces the uncertainty associated with the temperature of carbonate formation by several hundred meters.

Perhaps the most powerful aspect of this new technique is the ability to measure two variables that change with altitude, temperature and the $\delta^{18}O$ of surface water, in the same samples to estimate elevation. Paleosols deposited in the Bolivian Altiplano record both paleosol carbonate growth temperature and the $\delta^{18}O$ value of soil water that has been compared to the temperature lapse rate over land and the $\delta^{18}O$ values of meteoric water (Ghosh et al. 2006b). This two-variable approach to estimating elevation compares the temperature and water isotopic compositions determined from carbonates to the surface temperatures and rainfall isotopic compositions between mean annual and summertime extremes measured over an elevation transect in the Eastern Cordillera (**Supplemental Figure 4**; modern data for 1984 from Gonfiantini et al. 2001). This range of modern values is used, assuming that paleosols precipitate carbonate during or following the summer rainy season when plants are active and the rate of evapotranspiration is highest. The observation that paleosol carbonates plot within this range supports the inferred timing of their formation. Paleoelevation is determined from the intersection of paleosol temperatures/isotopic compositions with elevation contours that connect the mean annual and summertime extremes (Ghosh et al. 2006b).

Application to Paleoelevation Studies

Stable isotopes have recently been applied in a number of paleoelevation studies in the western North American Cordillera and Rocky mountains (Drummond et al. 1993, Norris et al. 1996, Dettman et al. 2000, Morrill & Koch 2002, Fricke 2003, Mulch et al. 2004, Sjostrom et al. 2006), New Zealand Alps (Chamberlain et al. 1999), the Sierra Nevada (Poage & Chamberlain 2002, Horton et al. 2004, Mulch et al. 2006), Basin and Range of the western United States (Horton & Chamberlain 2006), Himalaya and Tibetan Plateau (Garzione et al. 2000a,b; Rowley et al. 2001; Currie et al. 2005; Cyr et al. 2005; Rowley & Currie 2006), Cascades (Takeuchi & Larson 2005, Kohn et al. 2002), Patagonia (Blisniuk et al. 2005), and northern Andean Altiplano (Garzione et al. 2006, Ghosh et al. 2006b). Two general approaches have been taken to measure the relief associated with mountain ranges. One approach examines the isotope record in authigenic minerals deposited in basins on the leeward side of mountains, assuming that orographic precipitation associated with the topography that an airmass travels over leads to fractionation that is recorded in the basin despite its low elevation (Chamberlain et al. 1999, Chamberlain & Poage 2000, Kohn et al. 2002, Blisniuk et al. 2005). This technique aims to determine the existence of an orographic barrier associated with the mountain range by simply measuring changes in the isotopic composition recorded in authigenic minerals deposited in the basin fill as a function of time. This so-called rainshadow effect is assumed to

produce a decrease in the $\delta^{18}O$ and δD values recorded by authigenic minerals as relief increases, whereas an increase in $\delta^{18}O$ and δD values would reflect a decrease in relative relief. This approach is fraught with large uncertainties on quantitative estimates of paleoelevation because the convolution of orography, hypsometry, and precipitation amount results in nonunique correlation of orographic barrier elevation and isotopic composition. There is also the potential for sufficient precipitation to bypass an orographic barrier if the orographic barrier is not sufficiently long relative to the trajectory of storm tracks to actually preclude precipitation from sweeping around the barrier, thus negating the rainshadow effect. Another potential problem with this approach arises where the barrier is sufficiently large as to impact large-scale circulation, as happens in the Pamir-Karakoram region, such that precipitation on either side is derived from different sources and hence does not reflect the interposition of the orographic barrier. This is particularly problematic where the isotopic compositions on either side of the orographic barrier happen to be essentially the same. For example, application of this approach in the case of the western Tibetan plateau would imply that the plateau does not exist, as New Delhi (−5.81‰) is not significantly different from Hetian (−4.66‰) using 2001 IAEA-GNIP data on either side of the plateau.

A second approach examines high-elevation plateaus and associated mountain belts by measuring the isotopic composition of authigenic minerals deposited in intermontane basins. Precipitation falling at elevation must have been orographically lifted, and hence should be expected to have undergone Rayleigh distillation, as discussed above. At high elevations the magnitude of fractionation, relative to adjacent low-altitude precipitation is expected to be large, and hence the signature of paleotopography should be clear, irrespective of uncertainties in temperature and other parameters discussed above. Quantitative estimates of paleoaltitude with associated uncertainties are possible using this approach (Rowley et al. 2001; Garzione et al. 2000a,b, 2006; Currie et al. 2005; Rowley & Currie 2006). Rowley et al. (2001), Currie et al. (2005), and Rowley & Currie (2006), using modern surface water and precipitation data from regions north of the high Himalayan peaks, demonstrate that a close correlation exists between isotopic composition and predicted elevation. Thus modern surface water isotopic compositions reflect the plateau surface elevation, not the peak elevation of the range that bounds the plateau (e.g., Garzione et al. 2000a, Currie et al. 2005, Garzione et al. 2006, Rowley & Curry 2006). This conclusion is supported by numerous surface water and rainfall data sets showing that the isotopic composition of water reflects the typical depletion in transects from lower to higher elevation even on the leeward side of mountains (e.g., Friedman et al. 1992, Smith et al. 1979, Yonge et al. 1989, Blisniuk et al. 2005). Although the rainshadow effect can be significant in humid climates, such as the Cascades and the Southern Alps of New Zealand, and in the immediate rainshadow (within several tens of kilometers) of the mountains, this effect diminishes dramatically away from the mountains on the leeward side, probably as a result of (*a*) mixing with less ^{18}O-depleted vapor masses that were derived from different sources and/or traveled around the high topography and (*b*) below cloud-base evaporation from raindrops in the arid environment created by the rainshadow (e.g., discussions in Smith et al. 1979, Yonge et al. 1989).

To evaluate which of these approaches is applicable, it is necessary to examine modern patterns of precipitation (i.e., the vapor transport pathway and amount of precipitation) and the isotopic composition of surface waters and/or rainfall in the region of interest. In addition, application of elevation proxies independent of the isotopic composition of precipitation can bolster the interpretation of the elevation history. In the following section, we focus on the latter approach by examining the elevation records from the Himalaya/Tibetan plateau and the Andean plateau. Both the Himalaya and Andean plateau have elevation histories that are supported by multiple proxies, increasing the confidence in these records.

HIMALAYAS AND TIBETAN PLATEAU

The Himalayas and Tibetan plateau (**Figure 10**) represent the type example of continent-continent collision (Argand 1924, Bird & Dewey 1970). Recent reviews of the evolution of Tibet and the Himalayas (Burchfiel & Royden 1991, Copeland 1997, Dewey et al. 1988, Fielding 1996, Harrison et al. 1992, Molnar et al. 1993) emphasize the importance of topography as (*a*) a monitor for collision dynamics (Molnar et al. 1993), (*b*) a measure of crustal mass balance (Dewey et al. 1989, England & Housemann 1986, LePichon et al. 1992, Richter et al. 1992), (*c*) a significant influence on the local and global climate (Kutzbach et al. 1993, Ramstein et al. 1997, Raymo

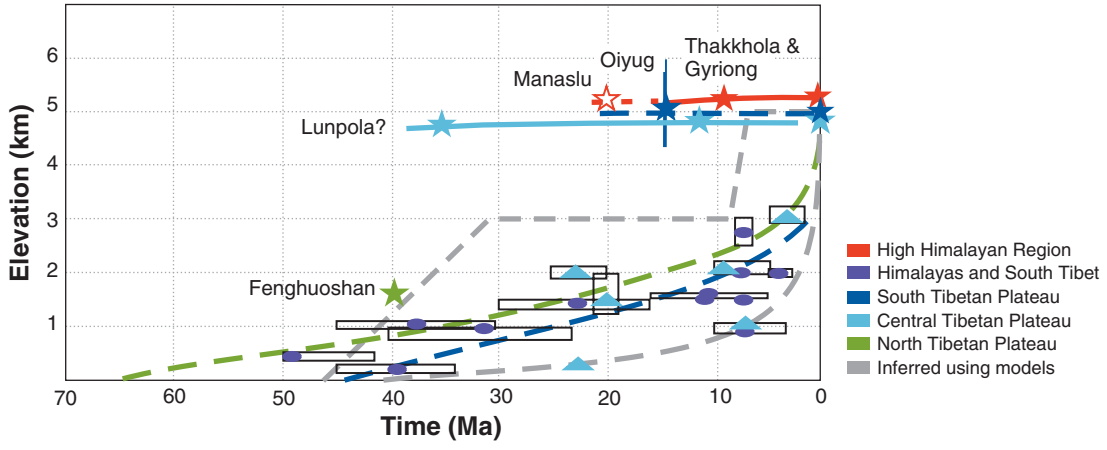

Figure 10

Summary of paleoelevation evolution of the Himalayas (*red*) and southern (*dark blue*), central (*light blue*), and northern (*green*) Tibet plateau based primarily on fossil faunal and floral data [see *ovals*, *triangles*, and stratigraphic ranges (*boxes*) from Mercier et al. (1987)]. The horizontal dimension of the boxes represents uncertainty of age, and the vertical dimension estimated uncertainty of elevation. Dashed lines represent previous estimates of the elevation history. Solid lines represent elevation histories constrained by isotoped-based paleoaltimetry. The upper gray curve is a generalized curve reflecting crust and mantle lithosphere thickening followed by convective removal of the mantle lithosphere at approximately 8 Ma based on England & Houseman (1986) and Molnar et al. (1993). The lower gray curve is based on faunal and floral interpretations as in Mercier et al. (1987).

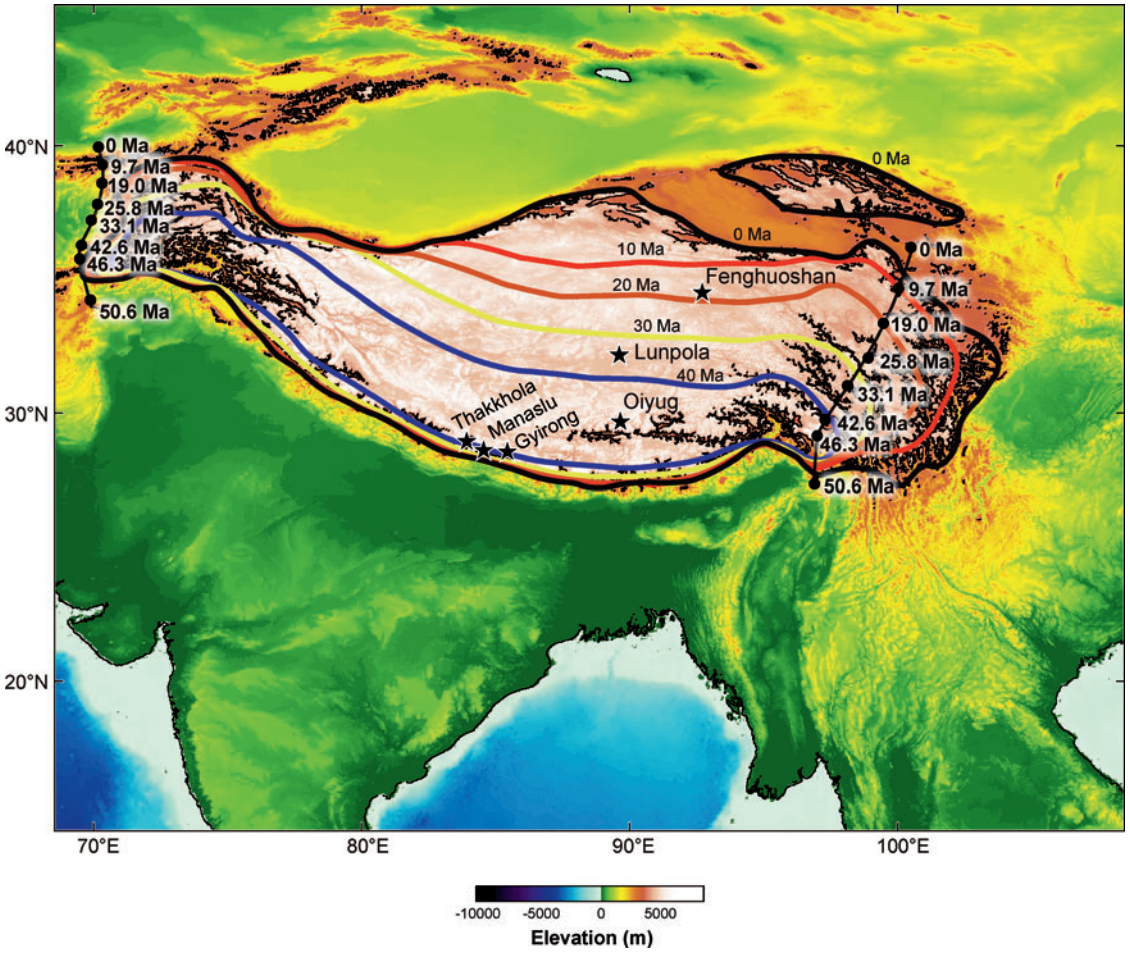

Figure 11

Himalaya and Tibetan plateau locations from which paleoelevation estimates have been published. Retrodicted size of the plateau above 4000 m as a function of time derived by scaling India-Asia convergence as discussed by Rowley & Currie (2006).

& Ruddiman 1992), and (*d*) a potential influence on ocean (Edmonds 1992, Richter et al. 1992) and atmospheric chemistry (Raymo 1991). Existing interpretations of the evolution of the topography of the Himalayas-Tibet range from suggestions of very large-scale uplift of much of Tibet in the last few million years (Mercier et al. 1987, Xu 1981) (**Figure 11**) to suggestions that significant topography predated the initiation of the collision of India with Asia (England & Searle 1987, Murphy et al. 1997).

Within the past six or so years, considerable progress has been made in obtaining and interpreting paleoelevation estimates from various basins of various ages within

the Himalayas and across the Tibetan plateau. It is important to specifically emphasize at the outset that the existing data remain sparse and therefore they can provide only an initial hint at potential conclusions regarding the paleoelevation evolution of this region and also the various modes of strain accommodation across this orogen. The data thus far are intriguing and suggest that considerable potential exists to verify and further validate the preliminary interpretations described below.

HIMALAYAS

Several data sets have been used to estimate the paleoelevation history of the Himalayas south of the Indus-Yarlung Tsangpo suture. From classic geomorphology, the simple observation is that the drainage divide between rivers flowing southward and those feeding the Indus and Yarlung (= Brahmaputra) rivers lies well north of the high peaks (Gansser 1964) (**Figure 9*a***). Of course, both the Indus and Yarlung also drain southward across the high Himalayas through the two deepest gorges in this mountain range. The obvious inference derived from these antecedent rivers is that the topography of the high Himalayas has grown subsequent to that of southernmost Tibet. The long history of Himalaya- and Tibet-derived sediments associated with these antecedent drainages (see summary in Rowley 1996) implies that a southward topographic slope has existed for at least 40 million years. This is based most clearly on the thick Eocene and Oligocene siliclastic sediments preserved in the Indo-Burman ranges [Disang and Barail Formations (Bender 1983)] that extend southward in the trench-fill materials exposed in the Andaman, Mentawai and Nicobar islands. Comparable relations exist in Afghanistan and western Pakistan, where thick turbiditic sequences of the Katawaz and Makran basins are exposed (see Rowley 1996 and references therein).

Quantitative estimates of the paleoelevation history of the Himalayas also have a long history, reflecting the significance of this information in constraining our understanding of the tectonics of this orogen (see Mercier et al. 1987). Most estimates have been derived from examining the altitude ranges of nearest living relatives (NLRs) of fossil plant and animal taxa found within intermontane basin deposits in the Himalayas and Tibet. **Figure 11** shows interpreted paleoelevation histories based on the NLR approach. From this approach, the high Himalayas have almost universally been interpreted to have remained at quite low elevations (<1 km) prior to the last 1 to 2 million years, at which time they are required to rise to their current highly elevated stature (Mercier et al. 1987). Molnar & England (1990) questioned this approach, pointing out that the primary controller on the altitude range of plants, in particular, is temperature and not altitude directly. Molnar & England (1990) thus pointed to the confounding effects of relatively recent climate cooling that has potentially significantly reduced altitude ranges of modern NLRs. The effect of this recent cooling is to imply significantly lower elevations based on this approach.

Perhaps the first stable isotope-based indication that the high Himalayas were highly elevated was presented by France-Lanord et al. (1988). They found strongly depleted δ^2H of some micas, particularly unchloritized biotite in both the massive Manaslu leucogranite and Chhokang Arm to argue for moderate temperature

infiltration of meteoric waters that altered biotites but not quartz, feldspar, or tourmaline. If alteration occurred at T ≈ 300°C these biotite compositions would correspond with waters with δ^2H_{mw} of approximately −180‰ to −215‰. Assuming low altitude precipitation with a δ^2H_p of approximately −40‰, then these depleted waters correspond with a $\Delta(\delta^{18}O_{mw})$ of approximately −20.9 ±2.0‰ (**Table 1**). According to the model, these compositions correspond with precipitation falling at between 5800 m to 6300 m elevation. Based on these micas, the paleoelevation in the Manaslu region is retrodicted to have been approximately 6100 m (France-Lanord et al. 1988) at about 20 Ma (Harrison et al. 1999) (**Figure 10**). This is comparable to present elevations in this region.

More recently, Garzione et al. (2000a,b) and Rowley et al. (1999, 2001) presented interpretations based on carbonates of various origins preserved within sedimentary rocks of the Thakkhola and Gyirong basins. Both the Thakkhola and Gyirong basins are associated with east-west extensional structures within the high peaks region of the Himalayas. Basin strata range from late Miocene (~10 Ma) to Pleistocene age (Garzione et al. 2000a, Wang et al. 1996) and contain paleosol carbonates, carbonate shells, and lacustrine limestones (**Table 1**). Normalizing oxygen isotopic compositions from Gyirong and Thakkhola basins with Bakiya Khola and Surai Khola paleosol carbonates imply a median elevation for the water contributing to these basin of 5200 m (**Table 1**) plotted in **Figure 11**.

Existing isotope-based paleoaltimetry in the Himalayas implies that there has been no recognizable change in the height of the high Himalaya since approximately 20 Ma. This is completely consistent with expectations based on evidence of timing of deformation and existence of a significant influx of sediments into adjacent basins throughout this interval. Unfortunately, it is not clear that it will be possible to extend this record significantly deeper in time, as older potential repositories are not obvious.

TIBETAN PLATEAU

Several data sets have recently been published that begin to hint at aspects of the paleoelevation history of the Tibetan Plateau. Unfortunately, existing data remain spatially sparse and as yet have limited temporal spans. Existing data are reviewed below from south to north across the plateau.

The Oiyug Basin is situated approximately 60 km north of the Indus-Yarlung Tsangpo suture in southern Tibet (**Figure 10**) within an extensional basin superimposed on arc-related Gandese plutonic and Linzizong volcanics. The basin includes waterlain tuffs deposited within a lacustrine setting that entomb a diverse flora, which has been investigated by Spicer et al. (2003), and pedogenic carbonates, described by Currie et al. (2005). The flora is sufficiently diverse that Spicer et al. (2003) could employ the Forest et al. (1999) paleoenthalpy approach to estimate the implied paleoelevation. Their best estimate of the paleoelevation is 4650 ± 875 m. Spicer et al. (2003) constrain the flora to be approximately 15.1 Ma old based on isotopically dated volcanic ashes bracketing the flora above and below. Pedogenic calcium carbonate nodules have average $\delta^{18}O_c$ values of –19.6‰ (**Table 1**). Model results indicate that

Table 1 Results from Tibet paleoaltimetry studies

	Age	δ^{18}Oc or δ^{2}H biotite (‰)	$\Delta(\delta^{18}O_{mw})$ (‰)	Uncertainty in $\Delta(\delta^{18}O_{mw})$ (‰)	Paleoelevation (m)	Uncertainty in mean estimated paleoelevation (m)	Paleoelevation Uncertainty from T & RH (1σ)	References
Himalayas								
Manaslu and Chokang Arm	20	−180 to −215	−20.9	2.5	6100	+290/−320	+1320/−890	France-Lanord et al. 1988
Thakkhola Graben	<10.0	−12.5 to −23.4	−6 to −17	2.8	5300	+430/−520	+1350/−670	Garzione et al. 2000a,b; Rowley et al. 2001
Gyirong Basin	≤7	−10.9 to −21.5	−5 to −15	2.8	5000	+480/−600	+1290/−590	Rowley et al. 2001
Southern Tibet								
Oiyug Basin	15.1	−19.6	−14.5	2.1	5200	+340/−390	+1330/−630	Currie et al. 2005
Central Tibet								
Lunpola Basin Dingqing	~10	−1.3 to −14.6	−10	2.0	4250	+460/−560	+1120/−520	Rowley & Currie 2006
Lunpola Basin Upper Nuibao	~35	−17.2	−12.6	2.0	4850	+370/−440	+1270/−570	Rowley & Currie 2006
Lunpola Basin Middle Nuibao	~39	−3.1 to −13.8	−9.2	2.0	4050	+500/−600	+1060/−500	Rowley & Currie 2006
Northern Tibet								
Fenghuoshan Group	~37	−10.3 to −11.7	−3.7	2.0	<2000	+850/−1050	+490/−360	Cyr et al. 2005

the southern Tibetan plateau achieved paleoelevations of ~5200 +1330/–630 m by at least 15 Ma (**Figure 11**). Our results are identical within uncertainty to those of Spicer et al. (2003) based on Oiyug Basin fossil floral physiognomy.

The Lunpola Basin is primarily a Tertiary sedimentary basin situated in the central part of the Tibetan plateau (**Figure 10**). The basin lies approximately halfway between the Qaidam Basin on the north and the Himalayas on the south. The Cenozoic strata of the Lunpola Basin are more than 4000 m thick and consist of two primary stratigraphic units: the Paleocene-Oligocene Niubao Formation and the Miocene-Pliocene Dingqing Formation. Rowley & Currie (2006) report results from lacustrine and paleosol carbonates from the middle and upper Niubao Formation of Eocene and Late Eocene-Early Oligocene age, respectively, as well as lacustrine marls and micritic limestones from the Miocene age middle Dingqing Formation (**Table 1**). The most depleted samples from the middle Dingqing Formation yield a $\Delta(\delta^{18}O_w)$ of $-10.0 \pm 2.0‰$ implying a paleoelevation of 4260 m +460/−560 m (**Figure 11**).

Abundant micritic $CaCO_3$ nodules from stacked argillic calcisols in the upper Niubao Formation yield $\delta^{18}O_c$ that averages $-17.2‰ \pm 1.2‰$ (2σ). The mean $\Delta(\delta^{18}O_w)$ for these samples is $-12.6 \pm 1.2‰$ (2σ), corresponding with a predicted mean elevation of the basin at approximately 4850 m +370/−440 m. Middle Niubao Formation thin-bedded lacustrine limestones and marls, the most negative of which yield $\Delta(\delta^{18}O_w)$ of approximately $-9.2 \pm 2.0‰$, correspond with estimates of paleoelevation for this sequence of approximately 4050 m +500/−600 m (**Table 1** and **Figure 11**).

Oxygen isotope-based estimates of paleoaltitude from the late Eocene-Oligocene Niubao Formation and Miocene middle Dingqing Formation of central Tibet indicate that the central Tibetan plateau has been characterized by elevations in excess of 4 km since 35 ± 5 Ma. These data are currently the oldest quantitative estimates and they imply a protracted history of a plateau at its current stature (Rowley & Currie 2006).

Oxygen and carbon isotopes together with Mg/Ca ratios of Eocene-Oligocene lacustrine carbonates from the Fenghuoshan Group of Hoh Xil basin in north-central Tibet (Cyr et al. 2005) have also been examined for their paleoelevation implications (**Figure 10**). This combined approach implies that the lakes were not significantly impacted by evaporitic re-enrichment of the oxygen isotopes. Applying the model to the isotopic data from Fenghuoshan carbonates (Cyr et al. 2005) implies that the hypsometric mean elevation of the drainage basins feeding Hoh Xil lakes $\leq$~2 km. In turn, this implies that the Hoh Xil basin, which is currently at an elevation of approximately 4700 m, was probably lower than 2000 m in the Eocene, and hence this region has undergone considerable (>2700 m) surface uplift in the past 39 Ma (**Figure 10**). Together with estimates of the Eocene paleoaltimetry from the Lunpola Basin to the south, these results provide the first suggestive evidence for differential uplift of the northern margin and northward growth of the Tibetan plateau. It should be pointed out that in the case of the Fenghuoshan carbonates, neither the trajectory of moisture nor a reasonable low-altitude sequence used to estimate $\Delta(\delta^{18}O_w)$ are clear. The Fenghuoshan is far removed today from the monsoon source of the Himalayas, and southern and Central Tibet and potentially from orographic precipitation in the

late Eocene to Oligocene. It is therefore not clear how well the isotopic compositions of this area will conform to the Rowley et al. (2001) model.

Paleoaltimetry data from southern and central Tibet, as well as from the Himalaya, imply that the elevation history of each of these regions is remarkably simple. In each of the basins, Thakkhola, Gyirong, Oiyug, and Lunpola, as well as from the Manaslu pluton, the data are consistent with an interpretation that they have remained elevated at about their current elevations for as long as the records extend. These data are contrary to models invoking significant (>1.5 km) contributions to the paleotopographic evolution from mantle lithosphere thickening concomitant with crustal thickening, followed by convective removal of the thickened mantle lithosphere (Molnar et al. 1993). Based on indirect interpretations, Molnar et al. (1993) inferred convective removal at approximately 8 Ma (**Figure 11**), whereas the existing paleoaltimetry data imply no discernible change in the past 20 Ma (Himalayas), 15 Ma (Oiyug Basin), and 35 $\pm$ 5 Ma (Lunpola Basin). Although the uncertainties are sufficiently large as to not preclude a kilometer or so of elevation change, the correspondence of each of these estimates with their present elevations implies that the most reasonable interpretation is that there has indeed been little variation, which is compatible with Airy isostatic compensation of an effectively doubled crustal thickness that has not changed much in the past 35 or so million years (Rowley & Currie 2006).

ANDEAN PLATEAU

The central Andean plateau is the second largest high plateau on Earth after the Tibetan plateau. The plateau has an average elevation of ~4 km and a width of up to ~400 km at the bend in the Andes near 18°S. In the central Andes, the plateau consists of ranges that flank the margins of the plateau, the Western and Eastern Cordilleras, and a region of internal drainage, called the Altiplano Basin (**Figure 12*a***). Peak elevations exceed 6 km in the cordilleras, whereas the Altiplano has an average elevation of ~3800 m. The Western Cordillera consists of a string of stratovolcanoes that represent the active magmatic arc, whereas the Eastern Cordillera is a fold-thrust belt that deforms Paleozoic metasedimentary rock. Most contractional deformation occurred in the Andean plateau between ~40 and 7 Ma (e.g., Elger et al. 2005, McQuarrie 2002).

Recent stable isotope data from the vicinity of Callapa on the Altiplano (Garzione et al. 2006, Ghosh et al. 2006b) support the longstanding argument that the Andean plateau has experienced significant post-10 Ma uplift, based on several lines of qualitative evidence (Isacks 1988, Gubbels et al. 1993, Kay et al. 1994, Kennan et al. 1997, Allmendinger, et al. 1997), and provide the first quantitative constraints on the timing and magnitude of late Miocene surface rise. Previous estimates of paleoelevation came from marine deposits in the Altiplano Basin and fossil leaf physiognomy (**Figure 12**). Shallow marine deposits indicate that the Altiplano lay at sea level at the end of the Cretaceous (Sempere et al. 1997). Estimates of mean annual temperature derived from fossil leaf physiognomy in the northern Altiplano and Eastern Cordillera suggest paleoelevations of no more than a third of the plateau's modern average height at ~15 to 20 Ma (Gregory-Wodzicki 2000) and no more than half by

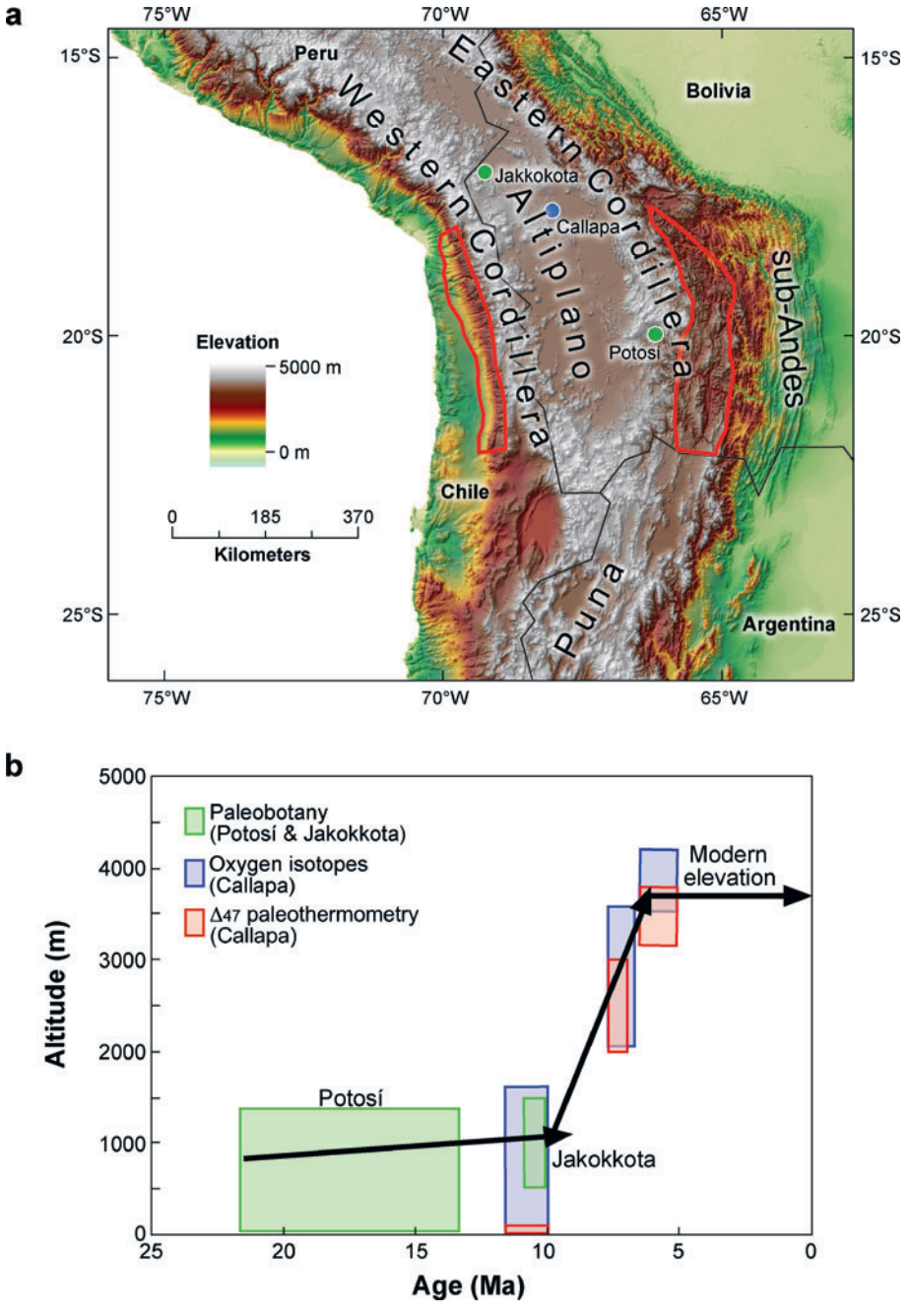

~10 Ma (Gregory-Wodzicki et al. 1998) (**Figure 12**). Stable isotope paleoelevation estimates from O isotopes (Garzione et al. 2006) and Δ_{47} paleothermometry (Ghosh et al. 2006b) suggest between 2.5 ± 0.5 km and 3.7 ± 0.4 km of surface uplift, respectively, between ~10 Ma and 6.8 Ma. In addition to quantitative proxies for surface uplift (**Figure 12*b***), geomorphic studies of the eastern and western flanks of the Andes allow for quantitative reconstructions of the relief generated during rotation and incision of low relief surfaces that developed prior to surface uplift (**Figure 12*a***) (Gubbels et al. 1993, Kennan et al. 1997, Hoke 2006). These studies indicate that 1 to 2 km of relief was generated along the flanks of the Andes, with age constraints on incision beginning between 9 and 5.5 Ma (Kennan et al. 1997, Farías et al. 2005, García & Hérail 2005, von Rotz et al. 2005, Kober et al. 2006, Schlunegger et al. 2006, Schildgen et al. 2006, Hoke et al. 2007). The correspondence in timing between incision along the flanks of the Andes and surface uplift of the Altiplano and Eastern Cordillera suggests regional surface uplift in the late Miocene that spanned the entire width of the Andean plateau over at least 5° latitude (Hoke & Garzione 2006).

Surface uplift of plateau regions requires both crustal thickening and removal of dense lower lithosphere. Crustal thickening of the Andean plateau occurred by faulting and folding observed in the upper crust (e.g., McQuarrie et al. 2002, Elger et al. 2005) and possibly by lower crustal flow (Husson & Sempere 2003, Hindle at al. 2005). Rapid surface uplift of several kilometers in ~3 ± 1 Myr over a large portion of the Andean plateau (**Figure 12**) cannot be generated by crustal shortening alone as the required shortening rate would be more than a factor of 3 larger than reconstructed shortening rates (Garzione et al. 2006). In addition, lower crustal flow alone cannot account for the simultaneous surface uplift of the Altiplano and the cordilleras because the relatively thick cordilleras would have been the source of lower crustal material that thickened the Altiplano (e.g., Husson & Sempere 2003). The magnitude, rapidity, and regional extent of late Miocene surface uplift require the removal of relatively dense eclogite and mantle lithosphere (Garzione et al. 2006). The viscosity coefficient required for convective removal of the lower lithosphere to generate surface uplift of this magnitude and rapidity is consistent with empirically derived flow laws for olivine and eclogite and produces reasonable estimates for both the required temperature of the Moho and mean stress within the mantle lithosphere (Molnar & Garzione 2007). The rapid removal of eclogitic lower crust and mantle

Figure 12

(*a*) Elevations of the Central Andean plateau between 15°S and 26°S, constructed with SRTM30 dataset. Regions outlined in red show the extent of middle-late Miocene low relief paleosurfaces that underwent rotation and incision beginning in late Miocene time. Green dots show locations of Miocene paleobotanical estimates of paleoelevation. Blue dot shows locations of late Miocene paleoelevation estimates from $\delta^{18}O$ and Δ_{47} of authigenic carbonates shown in (*b*). (*b*) History of elevation change from multiple proxies in the northern Altiplano and Eastern Cordillera. Black lines and arrows show trends in elevation over time. Paleobotany estimates from Gregory-Wodzicki et al. (1998) and Gregory-Wodzicki (2000), oxygen isotope estimates from Garzione et al. (2006), and Δ_{47} estimates from Ghosh et al. (2006).

lithosphere in the Andean plateau is supported by numerous lines of indirect evidence, including (*a*) geophysical constrains on the thermal and structural characteristic of the crust and mantle that suggest a crustal column of predominantly felsic composition, similar to upper crust (Beck & Zandt 2002), and the presence of hot asthenosphere below the Altiplano–Eastern Cordillera transition (Dorbath & Granet 1996, Myers et al. 1998); (*b*) the chemical characteristics of late Miocene to Pliocene mafic lavas in the southern Altiplano and Puna suggesting derivation from the mantle asthenosphere (Kay et al. 1994); and (*c*) high $^3He/^4He$ ratios across much of the Altiplano and Eastern Cordillera, interpreted to result from degassing of mantle-derived magmas (Hoke et al. 1994).

The similarities in paleoelevation estimates from standard stable isotope paleoaltimetry (**Figure 12*b***) and Δ_{47} paleothermometry are promising for efforts to measure paleoelevation with stable isotope applications, but the slight differences are equally intriguing. Ghosh et al. (2006b) use the two-variable technique described in New Directions in Carbonate Stable-Isotope Paleoaltimetry, above (**Supplementary Figure 4**), whereas Garzione et al. (2006) used the standard approach by calculating the isotopic composition of surface waters using the mean temperature estimates from Ghosh et al. (2006) to calculate elevation. Both techniques estimate a late Miocene elevation gain in the Altiplano in excess of ~2500 m to as much as 3700 m, representing most or possibly all of the modern elevation of the Altiplano (modern base level elevation = 3600 m to 3800 m). Comparison of the mean and range of estimates for each technique reveals that the two-variable approach produces lower estimates than the O isotope approach (**Figure 12**), and this difference becomes larger in older samples. There are several possible explanations for this difference. First, comparing the $\delta^{18}O$ values of waters to paleotemperature estimates derived from Δ_{47}, it is apparent older samples plot closer to the summer maximum temperatures and $\delta^{18}O$ values (**Supplementary Figure 4**). The most obvious explanations for the systematically lower elevation estimates from Δ_{47} are that the paleosols experienced minor burial diagenesis, soil water experienced evaporative enrichment of ^{18}O, or secular variations in temperature are larger than the secular variations in $\delta^{18}O$ values of meteoric waters associated with late Cenozoic global cooling. Ghosh et al. (2006b) suggest that minor diagenetic recrystallization during burial could increase temperature estimates by ~1 to 3°C, producing lower elevation estimates. Despite burial to depths of ~2.5 to 3.5 km for the 10.3 to 11.4 Ma samples in this study, there is no systematic increase in paleotemperature estimates with burial depth and age (Eiler et al. 2006), which suggests that burial diagenesis could not have had a major influence on Δ_{47} composition. Evaporative enrichment that produces a 1‰ increase in the $\delta^{18}O$ values of soil waters relative to a constant temperature of carbonate formation reduces elevation estimates derived from isoelevation lines by ~200 m at low elevations and <100 m at high elevations (**Supplementary Figure 4**). Perhaps the simplest explanation for lower elevation estimates based on Δ_{47} paleothermometry is that middle to late Miocene terrestrial temperatures were several degrees warmer than expected based on global climate change and changes in the latitude of South America (Ghosh et al. 2006b). If terrestrial temperature were relatively higher than estimates while the $\delta^{18}O$ of meteoric water was similar to modern at low elevation, then calculations

using both variables would underestimate the paleoelevation. This explanation can account for both the lower elevation estimates and the deviation of the older paleosol data to values closer to the summertime extreme emperatures. Despite differences in surface uplift estimates derived from different techniques, the comparison of multiple proxies indicates that most of the elevation gain ($\geq$2.5 km) occurred in the Altiplano between $\sim$10.3 and 6.8 Ma. A significant improvement in the accuracy and uncertainty of these estimates could come from establishing a low altitude climate record from the sub-Andean foreland that constrains the terrestrial temperature and isotopic composition of source moisture.

CONCLUSIONS

Paleoaltimetry has made considerable progress since 1998 when Chase et al. (1998) reviewed the field. We have primarily focused on stable isotope-based approaches to paleoaltimetry. This is not to imply that developments in other areas are less significant, but rather that it is now difficult to give sufficiently adequate coverage of all methods. The simple one-dimensional thermodynamic model of Rowley et al. (2001) provides a framework for understanding the relationship between stable isotopes and elevation. Comparison of transects of precipitation with elevation demonstrates that the model yields good fits to observations, particularly if local temperature and relative humidity conditions are employed. Even using the global mean T and RH for low latitudes, data misfits by less than 500 m, suggesting that for most paleoelevation purposes using global mean curve is reasonable.

Surface water isotopic compositions reflect the combined influences of variations in isotopic composition of precipitation as a function of elevation, amount of precipitation as a function of elevation, and drainage basin hypsometry above the sample elevation. Surface waters thus integrate over the catchment and should be thought of as recording the precipitation amount-weighted hypsometric mean elevation of the catchment. Because the amount of precipitation, and typically area, decreases with elevation, surface water isotopic compositions are strongly weighted toward recording relatively low elevations. It is difficult to see how to robustly interpret these data in terms of estimating the full hypsometry of such catchments, and thus deriving estimates of paleoelevations of adjacent mountains from measurement of the isotopic compositions derived from, for example, foreland basin fluvial or lacustrine sedimentary sequences. Evaporation of surface water samples, particularly in lacustrine settings can be significant with the consequent reenrichment of the waters, resulting in an underestimate of paleoelevations.

The recent development and application of multiply substituted C and O isotopes in carbonate represent an exciting new addition to the stable isotope arsenal for paleoaltimetry. Δ_{47} provides both a direct estimate of the temperature of equilibration between carbonate and water with a precision of $<\pm 3^{\circ}$C, significantly less than the $\pm 10^{\circ}$C typically assumed in calculations of carbonate water fractionation. This additional information thus can play a major role in reducing uncertainties in paleoelevation estimates. In addition, Δ_{47}-estimated paleotemperatures can be used to independently estimate paleoelevation through some assumption regarding

terrestrial lapse rates of temperature. Where agreement exists between estimates derived from $\Delta(\delta^{18}O_w)$ and Δ_{47}, confidence increases in these results. Finally, Δ_{47} temperatures can assist in identifying potential diagenetic overprints by indicating temperatures significantly higher than reasonable for surface temperatures (i.e., $T > 35$ to 40°C).

Application of stable isotope-based paleoaltimetry to the Himalayas, Tibet, and Andes, as reviewed above, is beginning to elucidate the evolution of paleotopography in these important orographic systems. These and associated approaches have been applied to other regions as well, including the Western Cordillera of North America, the southern Alps of New Zealand, and Patagonia. These data are beginning to yield significant insights into the process controlling orogenesis (sensu stricto). It is still very early in the development and application of these new techniques, but given the recent progress, we look forward to what we suspect will be an increasing number of data sets that will provide insights into the paleoelevation histories of mountain belts. These in turn should provide the basis to test existing ideas and hopefully spur new thinking into the underlying dynamic coupling of tectonics, elevation, surface processes, and climate.

ACKNOWLEDGMENTS

Drs. Rowley and Garzione would like to thank the many participants at the 2005 paleoelevation workshop at Lehigh University for helpful discussions that stimulated thinking about some of the themes in this review. In particular, we thank Andreas Mulch, Page Chamberlain, Matt Kohn, and Henry Fricke for discussions about applications in stable isotope paleoaltimetry. This research was supported in part by the National Science Foundation through grants EAR-9973222 and EAR-0609782 to D.B. Rowley and EAR-0230232 to C.N. Garzione.

LITERATURE CITED

Allmendinger RW, Jordan TE, Kay SM, Isacks BL. 1997. The evolution of the Altiplano-Puna plateau of the central Andes. *Annu. Rev. Earth Planet Sci.* 25:139–74

Ambach W, Dansgaard W, Eisner H, Mollner J. 1968. The altitude effect on the isotopic composition of precipitation and glacier ice in the Alps. *Tellus* 20:595–600

Anders AM, Roe GH, Hallet B, Montgomery DR, Finnegan N, Putkonen J. 2006. Spatial patterns of precipitation and topography in the Himalaya. In *Tectonics, Climate, and Landscape Evolution*, ed. SD Willett, N Hovius, M Brandon, DM Fisher, Geol. Soc. Am. Spec. Pap. 398, pp. 39–53. Boulder, CO: Geol. Soc. Am.

Argand E. 1924. *La Tectonique de L'Asie*. Presented at Proc. Int. Geol. Congr., XIIIth, Brussels

Beck SL, Zandt G. 2002. The nature of orogenic crust in the central Andes. *J. Geophys. Res.* 107(B10): doi:10.1029/2000JB000124

Beerling DJ, Royer DL. 2002. Fossil plants as indicators of the Phanerozoic global carbon cycle. *Annu. Rev. Earth Planetary Sci*. 30:527–56

Bender F. 1983. *Geology of Burma*. Berlin: Gebrüder Borntraeger. 293 pp.

Bigeleisen J, Mayer MG. 1947. Calculation of equilibrium constants for isotopic exchange reactions. *J. Chim. Phys*. 15:261–67

Bird JM, Dewey JF. 1970. Lithosphere plate-continental margin tectonics and evolution of Appalachian orogen. *Geolog. Soc. Am. Bull*. 81:1031–60

Blisniuk PM, Stern LA. 2005. Stable isotope paleoaltimetry—a critical review. *Am. J. Sci*. 305:1033–74

Blisniuk PM, Stern LA, Chamberlain CP, Idleman B, Zeitler PK. 2005. Climatic and ecologic changes during Miocene surface uplift in the southern Patagonian Andes. *Earth Planet. Sci. Lett*. 230:125–42

Burbank DW, Blythe AE, Putkonen J, Pratt-Sitaula B, Gabet E, et al. 2003. Decoupling of erosion and precipitation in the Himalayas. *Nature* 426:652–55

Burchfiel BC, Royden LH. 1991. Tectonics of Asia 50 years after the death of Emile Argand. *Eclogae Geol. Helv*. 84:599–629

Cerling TE, Quade J. 1993. Stable carbon and oxygen isotopes in soil carbonates. In *Continental Indicators of Climate*, ed. P Swart, KC Lohmann, JA McKenzie, S Savin, Proc. Chapman Conf., Am. Geophys. Union Monogr. 78, pp. 217–31. Jackson Hole, WY: Am. Geophys. Union

Cerling TE, Wang Y. 1996. Stable carbon and oxygen isotopes in soil CO_2 and soil carbonate; theory, practice, and application to some prairie soils of upper midwestern North America. In *Mass Spectrometry of Soils*, ed. TW Boutton, S Yamasaki, pp. 113–32. New York: Marcel Dekker

Chamberlain CP, Poage MA, Craw D, Reynolds RC. 1999. Topographic development of the Southern Alps recorded by isotopic composition of authigenic clay minerals, South Island. *N. Z. Chem. Geol*. 155:279–94

Chamberlain CP, Poage MA. 2000. Reconstructing the paleotopography of mountain belts from the isotopic composition of authigenic minerals. *Geology* 28:115–18

Chase CG, Gregory-Wodzicki KM, Parrish JT, DeCelles PG. 1998. Topographic history of the Western Cordillera of North America and controls on climate. In *Tectonic Boundary Conditions for Climate Reconstruction*, ed. TJ Crowley, KC Burke, pp. 73–97. New York: Oxford Univ. Press

Copeland P. 1997. The when and where of the growth of the Himalaya and the Tibetan Plateau. In *Tectonic Uplift and Climate Change*, ed. WF Ruddiman, pp. 19–40. New York: Plenum

Craig H. 1961. Isotopic variations in meteoric waters. *Science* 133:1702–8

Craig H, Gordon L. 1965. Deuterium and oxygen-18 variation in the ocean and the marine atmosphere. In *Stable Isotopes in Oceanographic Studies and Paleotemperatures*, ed. E Tongiorgi, pp. 9–130. Spoleto, Italy: Cons. Naz. Ric.

Crowley TJ, Burke KC, eds. 1998. *Tectonic Boundary Conditions for Climate Reconstructions*. Oxford: Oxford Univ. Press. 285 pp.

Currie BS, Rowley DB, Tabor NJ. 2005. Middle Miocene paleoaltimetry of southern Tibet: implications for the role of mantle thickening and delamination in the Himalayan orogen. *Geology* 33:181–84

Cyr A, Currie BS, Rowley DB. 2005. Geochemical and stable isotopic evaluation of Fenghuoshan Group lacustrine carbonates, north-central Tibet: implications for the paleoaltimetry of Late Eocene Tibetan Plateau. *J. Geology* 113:517–33

Dansgaard W. 1964. Stable isotopes in precipitation. *Tellus* 16:436–68

Dettman DL, Reische AK, Lohmann KC. 1999. Controls on the stable isotope composition of seasonal growth bands in aragonite fresh-water bivalves (unionidae). *Geochim. Cosmochim. Acta* 63:1049–57

Dettman DL, Lohmann KC. 2000. Oxygen isotope evidence for high altitude snow in the Laramide Rocky Mountains of North America during the late Cretaceous and Paleogene. *Geology* 28:243–46

Dettman DL, Kohn ML, Quade J, Ryerson FJ, Ojha TP, Hamidullah S. 2001. Seasonal stable isotope evidence for a strong Asian monsoon throughout the past 10.7 m.y. *Geology* 29:31–34

Dewey JF, Cande SC, Pitman WC. 1989. Tectonic evolution of the India/Eurasia collision zone. *Eclogae Geol. Helv*. 82:717–34

Dewey JF, Shackleton R, Chang CF, Sun YY. 1988. The tectonic evolution of Tibet. In *The Geological Evolution of Tibet*, pp. 379–413. London: R. Soc.

Dorbath C, Granet M. 1996. Local earthquake tomography of the Altiplano and the Eastern Cordillera of northern Bolivia. *Tectonophysics* 259:117–36

Drummond CN, Wilkinson BH, Lohmann KC, Smith GR. 1993. Effect of regional topography and hydrology on the lacustrine isotopic record of Miocene paleoclimate in the Rocky Mountains. *Palaeogeogr. Palaeoclimatol. Palaeoecol*. 101:67–79

Drummond CN, Patterson WP, Walker JCG. 1995. Climatic forcing of carbon-oxygen isotopic covariance in temperate-region marl lakes. *Geology* 23:1031–34

Duston NM, Owen RW, Wilkinson, BH. 1986. Water chemistry and sedimentological observations in Littlefield Lake, Michigan; implications for lacustrine marl deposition. *Environ. Geol. Water Sci*. 8:229–36

Edmonds J. 1992. Himalayan tectonics, weathering processes, and the strontium isotope record in marine limestones. *Science* 258:1594–97

Effler SW, Johnson DL. 1987. Calcium carbonate precipitation and turbidity measurements in Otisco Lake, New York. *Water Resour. Bull*. 23:73–79

Eiler JM, Garzione C, Ghosh P. 2006. Response to comment on "Rapid Uplift of the Altiplano Revealed Through ^{13}C–^{18}O Bonds in Paleosol Carbonates." *Science* 314:760c

Eiler JM, Schauble EA. 2004. $^{18}O^{13}C^{16}O$ in Earth's atmosphere. *Geochim. Cosmochim. Acta* 68:4767–77

Elger K, Oncken O, Glodny J. 2005. Plateau-style accumulation of deformation: Southern Altiplano. *Tectonics* 24: TC4020, doi:10.1029/2004TC001675.

England P, Housemann G. 1986. Finite strain calculations of continental deformation. II: Application to the India-Asia plate collision. *J. Geophys. Res*. 91:3664–76

England P, Searle MJ. 1987. The Cretaceous-Tertiary deformation of Lhasa block and its implications for crustal thickening in Tibet. *Tectonics* 5:1–14

Farías M, Charrier R, Comte D, Martinod J, Hérail G. 2005. Late Cenozoic deformation and uplift of the western flank of the Altiplano: evidence from the depositional, tectonic, and geomorphologic evolution and shallow seismic activity (northern Chile at 19°30'S). *Tectonics* 24:TC4001, doi:10.1029/2004TC001667

Fielding EJ. 1996. Tibet uplift and erosion. *Tectonophysics* 260:55–84

Forest C, Wolfe JA, Molnar P, Emanuel KA. 1999. Paleoaltimetry incorporating atmospheric physics and botanical estimates of paleoclimate. *Bull. Geolog. Soc. Am*. 111:497–511

France-Lanord C, Sheppard SF, Lefort P. 1988. Hydrogen and oxygen isotope variations in the High Himalaya peraluminous Manaslu leucogranite: evidence for heterogeneous sedimentary source. *Geochim. Cosmochim. Acta* 52:513–26

Fricke H. 2003. Investigation of early Eocene water-vapor transport and paleoelevation using oxygen isotope data from geographically widespread mammal remains. *Geol. Soc. Am. Bull*. 115:1088–96

Friedman I, ONeil JR. 1977. Compilation of stable isotope fractionation factors of geochemical interest. In *Data of Geochemistry*, ed. M Fleischer, pp. 12. Washington, DC: US Geol. Surv.

Friedman I, Smith GI, Gleason JD, Warden A. 1992. Stable isotope composition of waters in southeastern California: 1. Modern precipitation. *J. Geophys. Res*. 97:5795–812

Gansser A. 1964. *Geology of the Himalayas*. New York: Wiley Intersci. 289 pp.

García M, Hérail G. 2005. Fault-related folding, drainage network evolution and valley incision during the Neogene in the Andean Precordillera of Northern Chile. *Geomorphology* 65:279–300

Garzione CN, Dettman DL, Horton BK. 2004. Carbonate oxygen isotope paleoaltimetry: evaluating the effect of diagenesis on paleoelevation estimates for the Tibetan plateau. *Palaeogeogr. Palaeoclimatol. Palaeoecol*. 212:119–40

Garzione CN, Dettman DL, Quade J, DeCelles PG, Butler RF. 2000a. High times on the Tibetan Plateau: paleoelevation of the Thakkhola graben, Nepal. *Geology* 28:339–42

Garzione CN, Molnar P, Libarkin JC, MacFadden BJ. 2006. Rapid late Miocene rise of the Bolivian Altiplano: evidence for removal of mantle lithosphere. *Earth Planet. Sci. Lett*. 241:543–56

Garzione CN, Quade J, DeCelles PG, English NB. 2000b. Predicting paleoelevation of Tibet and the Himalaya from $d^{18}O$ vs altitude gradients in meteoric water across the Nepal Himalaya. *Earth Planet. Sci. Lett.* 183:215–29

Ghosh P, Adkins J, Affek H, Balta B, Guo W, et al. 2006a. ^{13}C–^{18}O bonds in carbonate minerals: a new kind of paleothermometer. *Geochim. Cosmochim. Acta* 70:1439–56

Ghosh P, Garzione CN, Eiler JM. 2006b. Rapid uplift of the Altiplano revealed through ^{13}C–^{18}O bonds in paleosol carbonates. *Science* 311:511–15

Gonfiantini R, Roche MA, Olivry JC, Fontes JC, Zuppi GM. 2001. The altitude effect on the isotopic composition of tropical rains. *Chem. Geol*. 181:147–67

Gregory KM. 1994. Paleoclimate and paleoelevation of the 35 Ma Florissant flora, Front Range, Colorado. *Paleoclimates* 1:23–57

Gregory-Wodzicki KM. 2000. Uplift history of the Central and Northern Andes: a review. *Geol. Soc. Am. Bull*. 112:1091–105

Gregory-Wodzicki KM, McIntosh WC, Velasquez K. 1998. Climatic and tectonic implications of the late Miocene Jakokkota flora, Bolivian Altiplano. *J. South Am. Earth Sci*. 11:533–60

Gubbels T, Isacks B, Farrar E. 1993. High level surfaces, plateau uplift, and foreland basin development, Bolivian central Andes. *Geology* 21:695–98

Harrison TM, Copeland P, Hall S, Quade J, Burner S, et al. 1993. Isotope preservation of Himalayan/Tibetan uplift denudation and climatic histories of two molasse deposits. *J. Geology* 101:157–76

Harrison TM, Copeland P, Kidd WSF, An Y. 1992. Raising Tibet. *Science* 255:1663–70

Harrison TM, Grove M, McKeegan KD, Coath CD, Lovera OM, Le Fort P. 1999. Origin and episodic emplacement of the Manaslu Intrusive Complex, Central Himalaya. *J. Petrol*. 40:3–19

Hindle D, Kley J, Oncken O, Sobolev S. 2005. Crustal balance and crustal flux from shortening estimates in the Central Andes. *Earth Planet. Sci. Lett*. 230:113–24

Hodell DA, Fahnenstiel GL, Robbins LL, Schelske CL. 1998. Biologically induced calcite and its isotopic composition in Lake Ontario. *Limnol. Oceanogr*. 43:187–99

Hoke GD. 2006. *The influence of climate and tectonics on the geomorphology of the western slope of the Central Andes, Chile and Peru*. PhD dissertation, Cornell Univ., New York. 283 pp.

Hoke GD, Garzione CN. 2006. *Late Miocene Plateau—wide surface uplift in the Central Andes: an integration of stable isotope paleoaltimetry and geomorphology*. Presented at Backbone Am.—Patagon. Alsk., 3–7 April 2006, Mendoza, Argent. (Abstr.)

Hoke GD, Isacks BL, Jordan TE, Blanco N, Tomlinson AJ, Ramezani J. 2007. Geomorphic evidence for post-10 Ma uplift of the western flank of the Central Andes (18°30'-22°S). *Tectonics*. Submitted

Horita J, Wesolowski DJ. 1994. Liquid-vapor fractionation of oxygen and hydrogen isotoopes of water from freezing to the critical temperature. *Geochim. Cosmochim. Acta* 58:3425–37

Hoorn C, Ojha T, Quade J. 2000. Palynological evidence for vegetation development and climatic change in the Sub-Himalayan Zone (Neogene, Central Nepal). *Palaeogeogr. Palaeoclimatol. Palaeoecol*. 163:133–61

Horton TW, Chamberlain CP. 2006. Stable isotopic evidence for Neogene surface downdrop in the Central Basin and Range Province. *Geol. Soc. Am. Bull*. 118:475–90

Horton TW, Sjostrom DJ, Abruzzese MJ, Poage MA, Waldbauer JR, et al. 2004. Spatial and temporal variation of Cenozoic surface elevation in the Great Basin and Sierra Nevada. *Am. J. Sci.* 304:862–88

Husson L, Sempere T. 2003. Thickening the Altiplano crust by gravity-driven crustal channel flow. *Geophys. Res. Lett*. 30(5):1243, doi:10.1029/2002GL016877

IAEA. 1992. *Statistical Treatment of Data on Environmental Isotopes in Precipitation*. Vienna: Int. At. Energy Agency. 781 pp.

Isacks BL. 1988. Uplift of the central Andean plateau and bending of the Bolivian orocline. *J. Geophys. Res*. 93:3211–31

Kalnay E, Kanamitsu M, Kistler R, Collins W, Deaven D, et al. 1996. The NCEP/NCAR 40-year reanalysis project. *Bull. Am. Meteorol. Soc.* 77:437–71

Kay SM, Coira B, Viramonte J. 1994. Young mafic back arc volcanic rocks as indicators of continental lithospheric delamination beneath the Argentine Puna plateau, Central Andes. *J. Geophys. Res*. 99:24323–39

Kennan L, Lamb S, Hoke L. 1997. High altitude paleosurfaces in the Bolivian Andes: Evidence for Late Cenozoic surface uplift. In *Paleosurfaces: Recognition, Reconstruction and Paleoenvironmental Interpretation*, ed. M Widdowson, *Geol. Soc. Spec. Publ. 120*, pp. 307–24. London: Geol. Soc.

Kim ST, O'Neil JR. 1997. Equilibrium and nonequilibrium oxygen isotope effects in synthetic carbonates. *Geochim. Cosmochim. Acta* 61:3461–75

Kober F, Schlunegger F, Zeilinger G, Schneider H. 2006. Surface uplift and climate change: the geomorphic evolution of the Western Escarpment of the Andes of northern Chile between the Miocene and present. In *Tectonics, Climate, and Landscape Evolution*, ed. SD Willett, N Hovius, MT Brandon, DM Fisher, Geol. Soc. Am. Spec. Pap. 398, pp. 75–86. Boulder, CO: Geol. Soc. Am.

Kohn MJ, Miselis JL, Fremd TJ. 2002. Oxygen isotope evidence for progressive uplift of the Cascade Range, Oregon. *Earth Planet. Sci. Lett.* 204:151–65

Kutzbach JE, Prell WL, Ruddiman WF. 1993. Sensitivity of Eurasian climate to surface uplift of the Tibetan Plateau. *J. Geology* 101:177–90

LePichon X, Fournier M, Jolivet L. 1992. Kinematics, topography, shortening and extrusion in the India-Eurasia collision. *Tectonics* 11:1085–98

Liu B, Phillips FM, Campbell AR. 1996. Stable carbon and oxygen isotopes of pedogenic carbonates, Ajo Mountains, southern Arizona: implications for paleoenvironmental change. *Palaeogeogr. Palaeoclimatol. Palaeoecol.* 124:233–46

Majoube M. 1971a. Fractionement en oxygen 18 et en deuterium entre l'eau et sa vapeur. *J. Chim. Phys.* 10:1423–36

Majoube M. 1971b. Fractionnement en ^{18}O Entre La Glace et La Vapeur D'Eau. *J. Chim. Phys.* 68:625–36

McKenzie JA. 1985. Stable-isotope mapping in Messinian evaporative carbonates of central Sicily. *Geology* 13:851–54

McKenzie JA, Hollander DJ. 1993. Oxygen isotope record in recent sediments from Lake Greiffen, Switzerland (1750–1986): application of continental isotopic indicator for evaluation of changes in climate and atmospheric circulation patterns. In *Continental Indicators of Climate*, ed. P Swart, KC Lohmann, JA McKenzie, S Savin, Proc. Chapman Conf., Am. Geophys. Union Monogr. 78, pp. 217–31. Jackson Hole, WY: Am. Geophys. Union

McElwain JC. 2004. Climate-independent paleoaltimetry using stomatal density in fossil leaves as a proxy for CO_2 partial pressure. *Geology* 32:1017–20

McQuarrie N. 2002. The kinematic history of the Central Andean fold-thrust belt, Bolivia; implications for building a high plateau. *Geol. Soc. Am. Bull.* 114:950–63

Mercier JL, Armijo R, Tapponier P, Carey-Gailhardis E, Han TL. 1987. Change from late Tertiary compression to Quaternary extension in southern Tibet during the India-Asia collision. *Tectonics* 6:275–304

Merlivat L, Nief G. 1967. Isotopic fractionation of solid-vapor and liquid-vapor changes of state of water at temperatures below 0°C. *Tellus* 19:122–27

Molnar P, England P. 1990. Late Cenozoic uplift of mountain ranges and global climate change: chicken or egg? *Nature* 346:29–34

Molnar P, England P, Martinod J. 1993. Mantle dynamics, uplift of the Tibetan Plateau, and the Indian Monsoon. *Rev. Geophys.* 31:357–96

Molnar P, Garzione CN. 2007. Bounds on the viscosity coefficient of continental lithosphere from removal of mantle lithosphere beneath the Altiplano and Eastern Cordillera. *Tectonics*. In press
Morrill C, Koch PL. 2002. Elevation or alteration? Evaluation of isotopic constraints on paleoaltitudes surrounding the Eocene Green River Basin. *Geology* 30:151–54
Mulch A, Graham SA, Chamberlain CP. 2006. Hydrogen isotopes in Eocene river gravels and paleoelevation of the Sierra Nevada. *Science* 313:87–89
Mulch A, Teyssier C, Cosca MA, Vanderhaeghe O, Vennemann TW. 2004. Reconstructing paleoelevations in eroded orogens. *Geology* 32:525–28
Murphy MA, Yin A, Harrison TM, Dürr SB, Chen Z, et al. 1997. Did the Indo-Asian collision alone create the Tibetan plateau? *Geology* 25:719–22
Myers SC, Beck S, Zandt G, Wallace T. 1998. Lithospheric-scale structure across the Bolivian Andes from tomographic images of velocity and attenuation for *P* and *S* waves. *J. Geophys. Res.* 103:21233–52
Nelson SV. 2005. Paleoseasonality inferred from equid teeth and intratooth isotopic variability. *Palaeogeogr. Palaeoclimatol. Palaeoecol.* 222:122–44
Norris RD, Jones LS, Corfield RM, Cartlidge JE. 1996. Skiing in the Eocene Uinta Mountains? Isotopic evidence in the Green River Formation for snowmelt and large mountains. *Geology* 24:403–6
Pierrehumbert RT. 1999. Huascaran δ18 O as an indicator of tropical climate during the Last Glacial Maximum. *Geophys. Res. Lett.* 26:1345–48
Poage MA, Chamberlain CP. 2001. Empirical relationships between elevation and the stable isotope composition of precipitation and surface waters: considerations for studies of paleoelevation change. *Am. J. Sci.* 301:1–15
Poage MA, Chamberlain CP. 2002. Stable isotopic evidence for a pre-middle Miocene rain shadow in the Western Basin and Range: implications for the paleotopography of the Sierra Nevada. *Tectonics* 21:doi 10.1029.2001TC001303
Putkonen JK. 2004. Continuous snow and rain data at 500 to 4400 m altitude near Annapurna, Nepal, 1999–2001. *Arct. Antarct. Alpine Res.* 36:244–48
Quade J, Cater JML, Ojha TP, Adam J, Harrison TM. 1995. Late Miocene environmental change in Nepal and the northern Indian subcontinent: stable isotopic evidence from paleosols. *Geol. Soc. Am. Bull.* 107:1381–97
Quade J, Cerling TE, Bowman JR. 1989. Development of Asian monsoon revealed by marked ecological shift during the latest Miocene in northern Pakistan. *Nature* 342:163–66
Ramesh R, Sarin MM. 1995. Stable isotope study of the Ganga (Ganges) river system. *J. Hydrol.* 139:49–62
Ramstein G, Fluteau F, Besse J, Joussaume S. 1997. Effects of orogeny, plate motion and land-sea distribution on Eurasian climate change over the past 30 million years. *Nature* 386:788–95
Raymo ME. 1991. Geochemical evidence supporting T.C. Chamberlin's theory of glaciation. *Geology* 19:344–47
Raymo MF, Ruddiman WF. 1992. Tectonic forcing of late Cenozoic climate. *Nature* 359:117–22
Bur. Geol. Mineral Res. Xizang Auton. Region. 1993. *Regional Geology of Xizang (Tibet) Autonomous Region*. Beijing: Geol. Publ. House. 707 pp.

Richter F, Rowley DB, DePaolo DJ. 1992. Sr isotope evolution of seawater: the role of tectonics. *Earth Planet. Sci. Lett*. 109:11–23
Roe GH. 2005. Orographic Precipitation. *Annu. Rev. Earth Planet. Sci*. 33:645–71
Roe GH, Montgomery DR, Hallet B. 2002. Effects of orographic precipitation variations on the concavity of steady-state river profiles. *Geology* 30:143–46
Rowley DB. 1996. Age of initiation of collision between India and Asia: A review of stratigraphic data. *Earth Planet. Sci. Lett*. 145:1–13
Rowley DB, Currie BS. 2006. Palaeo-altimetry of the late Eocene to Miocene Lunpola Basin, central Tibet. *Nature* 439:677–81
Rowley DB, Pierrehumbert RT, Currie BS. 2001. A new approach to stable isotope-based paleoaltimetry: implications for paleoaltimetry and paleohypsometry of the High Himalaya since the Late Miocene. *Earth Planet. Sci. Lett*. 188:253–68
Rowley DB, Pierrehumbert RT, Currie BS, Hosman A, Clayton RN, et al. 1999. Stable isotope-based paleoaltimetry and the elevation history of the High himalaya since the late Miocene. Geol. Soc. Am. Abstr. Progr.
Rozanski K, Sonntag C. 1982. Vertical distribution of deuterium in atmospheric water vapour. *Tellus* 34:135–41
Ruddiman WF, ed. 1997. *Tectonic Uplift and Climate Change*. New York: Plenum. 535 pp.
Sahagian D, Proussevitch A, Carlson W. 2002. Timing of Colorado Plateau uplift: initial constraints from vesicular basalt-derived paleoelevations. *Geology* 30:807–10
Sahagian DL, Maus JE. 1994. Basalt vesicularity as a measure of atmospheric pressure and paleoelevation. *Nature* 372:449–51
Schildgen TF, Whipple KX, Hodges KV, Pringle MS. 2006. Tectonics of the western margin of the Altiplano in Southern Peru from river incision history. *GV Int. Conf.*, Potsdam, p. 66. (Abstr.)
Schlunegger F, Zeilinger G, Kounov A, Kober F, Hüsser B. 2006. Scale of relief growth in the forearc of the Andes of Northern Chile (Arica latitude, 18°S). *Terra Nova*. 18:217–23
Sempere T, Butler RF, Richards DR, Marshall LG, Sharp W, Swisher CC III. 1997. Stratigraphy and chronology of Upper Cretaceous-lower Paleogene strata in Bolivia and Northwest Argentina. *Geol. Soc. Am. Bull* 109:709–27
Siegenthaler U, Oeschger H. 1980. Correlation of ^{18}O in precipitation with temperature and altitude. *Nature* 285:314–17
Sjostrom DJ, Hren HT, Horton TW, Waldbauer JR, Chamberlain CP. 2006. Stable isotopic evidence for an Early Tertiary elevation gradient in the Great Plains-Rocky-Mountain region. *Geol. Soc. Am. Spec. Pap*. 398:309–19
Smith GI, Friedman I, Klieforth H, Hardcastle K. 1979. Areal distribution of deuterium in eastern California precipitation, 1968–1969. *J. Appl. Meteorol*. 18:172–88
Spicer RA, Harris NBW, Widdowson M, Herman AB, Guo S, et al. 2003. Constant elevation of southern Tibet over the past 15 million years. *Nature* 421:622–24
Takeuchi A, Larson PB. 2005. Oxygen isotope evidence for the late Cenozoic development of an orographic rain shadow in eastern Washington, USA. *Geology* 33:313–16

Thompson LG, Mosley-Thompson E, Henderson KA. 2000. Ice core paleoclimate records in tropical South America since the Last Glacial Maximum. *J. Quat. Sci.* 15(4):377–94

Thompson LG, Mosley-Thompson E, Davis ME, Bolzan JF, Yao T, et al. 1989. 100,000 year climate record from Qinghai-Tibetan Plateau ice cores. *Science* 246(4929):474–477.

Urey HC. 1947. The thermodynamic properties of isotopic substances. *J. Chem. Soc.* 1947:561–81

von Rotz R, Schlunegger F, Heller F, Villa I. 2005. Assessing the age of relief growth in the Andes of northern Chile: Magneto-polarity chronologies from Neogene continental sections. *Terra Nova* 17:462–71

Wang FB, Li SF, Shen XH, Zhang J, Yan G. 1996. Formation, evolution and environmental changes of the Gyirong Basin and uplift of the Himalaya. *Sci. China (Series D)* 39:401–9

Wang Z, Schauble EA, Eiler JM. 2004. Equilibrium thermodynamics of multiply-substituted isotopologues of molecular gases. *Geochim. Cosmochim. Acta* 68:4779–97

Wolfe JA. 1993. A method for obtaining climate parameters from leaf assemblages. *U.S. Geol. Surv. Bull.* 1964:35

Xia JB. 1983. Cenozoic of Baingoin and its borders, Xizang (Tibet). *Contrib. Geol. Qinghai-Xizang (Tibet) Plateau* 3:243–54 (Chinese with English summary)

Xu R. 1981. Vegetational changes in the past and the uplift of Qinghai-Xizang plateau. In *Geological and Ecological Studies of Qinghai-Xizang Plateau*, ed. DS Liu, et al., pp. 139–48. Beijing: Sci. Press

Xu ZY. 1980. The Tertiary and its petroleum potential in the Lunpola Basin, Tibet. *Oil Gas Geol.* 1:153–58

Xu ZY, Zhao JP, Wu ZL. 1985. On the Tertiary continental basins and their petroleum potential in Qinghai-Xizang (Tibet) Plateau with Lunpola Basin as example. *Contrib. Geol. Qinghai-Xizang (Tibet) Plateau* 17:391–99 (Chinese with English summary)

Yonge CJ, Goldberg L, Krouse HR. 1989. An isotopic study of water bodies along a traverse of Southwestern Canada. *J. Hydrol.* 106:245–55

Annual Review of Earth and Planetary Sciences
Volume 35, 2007

Contents

Indexes

Errata

An online log of corrections to *Annual Review of Earth and Planetary Sciences* chapters (if any, 1997 to the present) may be found at http://earth.annualreviews.org